NTNU – Trondheim
Norwegian University of
Science and Technology

Magnetic Nanoparticles for Extraction of Naphthenic Acids from Model Oil

Mia Elise Ronander

Chemical Engineering and Biotechnology
Submission date: June 2015
Supervisor: Johan Sjöblom, IKP
Co-supervisor: Galina Rodionova, IKP

Norwegian University of Science and Technology
Department of Chemical Engineering

Preface

This thesis concludes my Master of Science degree at the Department of Chemical Engineering of Norwegian University of Science and Technology (NTNU). This project is based on a specialization project from the fall of 2014, and experimental work carried out at Ugelstad Laboratoy in the spring of 2015. The experimental work was performed under supervision of Professor Johan Sjöblom (main supervisor) and Dr. Galina Rodionova (co-supervisor).

I would like to thank my co-supervisor, Dr. Galina Rodionova, for great guidance, proof reading countless times and for being positive no matter what. I also want to thank Dr. Sébastien Simon, for teaching me everything I needed to know in the laboratory and for knowing the answer to all my questions. I am thankful to my main supervisor, Professor Johan Sjöblom, for giving me the opportunity to write this thesis.

Finally, I would like to thank my family, friends and Robin for love, support and for pushing me to do my best.

I declare that this is an independent work according to the exam regulations of the Norwegian University of Science and Technology (NTNU)

Trondheim 11.06.2015

Mia Elise Ronander

Abstract

The Master's thesis aims for synthesis of magnetic nanoparticles (MNP), silica-coated magnetic nanoparticles, and their application for extraction of naphthenic acids (NA) from model oil.

The present work is a part of a 2-year Post Doc project supported by a Vista program. The program is funded by Statoil and conducted in close collaboration with The Norwegian Academy of Science and Letters. The goal of the main project is to establish new methods for both preventing formation and facilitating removal of the NA. The newly developed methods will be based on the application of functionalized magnetic nanoparticles (FMN) for extraction of NA before formation of the metal naphthenates as well as their removal.

Commercial magnetic particles with silica cover (SiO_2-MAG) were purchased, which could be used just as they are or be directly functionalized. The particles were characterized by digital video microscopy (DVM) to estimate the size of the particles. The diameter was found to be 3,3 μm, and a specific surface area calculated to be 1,4 m^2/g. This area was too small for NA adsorption.

Therefore, synthesis of new nanoparticles was required. Fe_3O_4 MNP were obtained by co-precipitation, and coated with silica via a sol-gel approach. The synthesized MNP had magnetic properties, and were attracted when a magnetic field was applied. They were then characterized by gas adsorption analysis, which enabled the calculation of the specific surface area. The Fe_3O_4 MNP and Fe_3O_4/SiO_2 MNP had a large specific surface area of approximately 100 m^2/g, and the silica covered MNP were used for NA adsorption in octane. The size of the Fe_3O_4 MNP was estimated to be 12 nm by X-ray diffraction (XRD), and the analysis also confirmed a crystalline structure matching the theoretical Fe_3O_4 structure.

4-heptylbenzoic acid was used as a model NA and octane was used as model oil for adsorption experiments. A calibration curve for NA in octane was plotted, and adsorption of NA by MNP coated with silica was done to obtain an adsorption curve.

Sammendrag

Denne masteroppgaven retter seg mot syntese av magnetiske nanopartikler (MNP), silika dekkede MNP, og deres applikasjon for ekstraksjon av naftenske syrer (NA) fra modellolje.

Dette arbeidet er en del av et 2-årig Post Doc prosjekt som er støttet av et Vista program. Dette programmet er finansiert av Statoil og blir utført i nært samarbeid med Det Norske Videnskaps-Akademi. Målet for hovedprosjektet er å etablere nye metoder både for å forebygge og for fjerning av NA. De nyutviklede metodene vil være basert på bruken av funksjonaliserte magnetiske nanopartikler (FMN) for ekstraksjon av NA før dannelsen av metall naftenater (MeNA), så vell som deres fjerning.

Kommersielle silika dekkede MNP (SiO_2-MAG) ble kjøpt, og kan brukes som de er eller bli direkte funksjonalisert. Disse partiklene ble karakterisert med digital video mikroskopi (DVM) for å estimere partiklenes størrelse. Diameteren ble funnet til å være 3,3 μm, og det spesifikke overflatearealet ble beregnet til å være 1,4 m^2/g. Dette arealet var for lite for NA adsorpsjon.

Derfor var det nødvendig å syntetisere nye nanopartikler. Fe_3O_4 MNP ble syntetisert ved bruk av en utfellingssyntese (co-precipitation), og ble dekket med silika via en sol-gel tilnærming. De syntetiserte MNP hadde magnetiske egenskaper, og ble tiltrukket når et magnetisk felt ble tilført. Deretter ble de karakterisert ved gassadsorpsjonsanalyse, og gjorde det mulig å finne det spesifikke overflatearealet. Fe_3O_4 MNP og Fe_3O_4/SiO_2 MNP hadde stort overflateareal på omtrent 100 m^2/g, og Fe_3O_4/SiO_2 MNP ble brukt til adsorpsjon av NA fra oktan. Størrelsen av Fe_3O_4 MNP ble estimert til å være 12 nm med røntgendiffraksjon (XRD), og analysen bekreftet også en krystallinsk struktur som passer med den teoretiske Fe_3O_4 strukturen.

4-heptylbenzosyre ble brukt som modell NA og oktan ble brukt som modellolje for adsorpsjonseksperimenter. En kalibreringskurve for NA i oktan ble plottet, og adsorpsjon av NA med SiO_2/Fe_3O_4 MNP med silika ble utført for å danne en adsorpsjonskurve.

Abbreviations

AAIL	Amino acid ionic liquids
APDES	3-aminopropyl-ethyl-diethoxysilane
APES	3-aminopropyl-diethyl-ethoxysilane
API	American Petroleum Institute
APTES	3-aminopropyl-triethoxysilane
APTMS	Aminopropyltrimethoxysilane
BET	Brunauer-Emmett-Teller
CaNA	Calcium naphthenate
DLS	Dynamic light scattering
DVM	Digital video microscope
FMN	Functionalized magnetic nanoparticles
HPLC	High-performance liquid chromatography
LSS	Liquid-solid-solution reaction
MeNA	Metal naphthenate
MNP	Magnetic nanoparticles
NA	Naphthenic acids
ODS	Octadecyltriethoxysilane
TEOS	Tetraethyl orthosilicate
TAN	Total acid number

List of symbols

A	Absorbance
α	Constant in Freundlich isotherm
β	Line broadening at half the maximum intensity
C	Concentration
C_0	Initial concentration of adsorbate
C_e	Equilibrium concentration of the solute in the liquid
C_s	Concentration of solute when all layers (BET) are saturated
C_{solid}	Concentration of adsorbent
D	Diffusion coefficient
d	Interplanar spacing
D_e	Free liquid diffusivity
δ	Thickness of the diffusional sublayer
ε	Molar absorptivity
Γ	Surface excess
H	Magnetic field
I	Transmitted intensity
I_0	Intensity of incident light at given wavelength
K	Dimensionless shape factor
K_A	Adsorption rate constant divided by the desorption rate constant
K_B	Constant related to binding intensity for all adsorbed layers
k_B	Boltzmann constant

K_f	Mass transfer coefficient
$K_{w/o}$	Partitioning coefficient
Λ	Wavelength
M	Magnetization
$\bar{m}$	Volume-distributed moments
m	Mass
n	Constant in Freundlich isotherm
ŋ	Viscosity
q_e	Equilibrium concentration of a solute on the surface of an adsorbent
q_m	Maximum adsorbable value of a solute on the surface of an adsorbent
R_s	Radius of sphere
T	Temperature
τ	Mean size of the ordered crystalline domains
Θ	Bragg angle of incidence
V	Volume
w	Weight of solute adsorbed per unit weight of solid

Contents

1. Introduction

The natural occurring crude oil is an unrefined petroleum product which varies in composition from one oil field to another. The crude oil is a complex mixture of gaseous, liquid and solid hydrocarbons with small quantities of organic compounds containing nitrogen, oxygen, sulphur and trace amounts of metallic constituents (Speight, 1999). The naphthenic acids give rise to the high total acid number (TAN) of heavy crude oils, and are mostly part of the resin fraction (Aske, 2002).

1.1 Chemistry and interfacial behaviour of naphthenic acids

Naphthenic acids (NA) occur naturally in crude oils, and consist of a complex blend of alkyl-substituted acyclic and cycloaliphatic carboxylic acids. The mixture of NA consists of hundreds of components that have currently not been individually identified; hence there is not enough information about the structure of the NA. The acids are mainly found in immature heavy crude oils, and the TAN can be measured by potentiometric titration (Laredo, et al., 2004). The general chemical formula is $C_nH_{2n+Z}O_2$, where n indicates the carbon number and Z is zero if the molecule is a fatty acid, or negative depending on the number of condensed and/or aromatic rings (Clemente & Fedorak, 2005). Several structures are proposed in figure 1-1, with the corresponding chemical formulas.

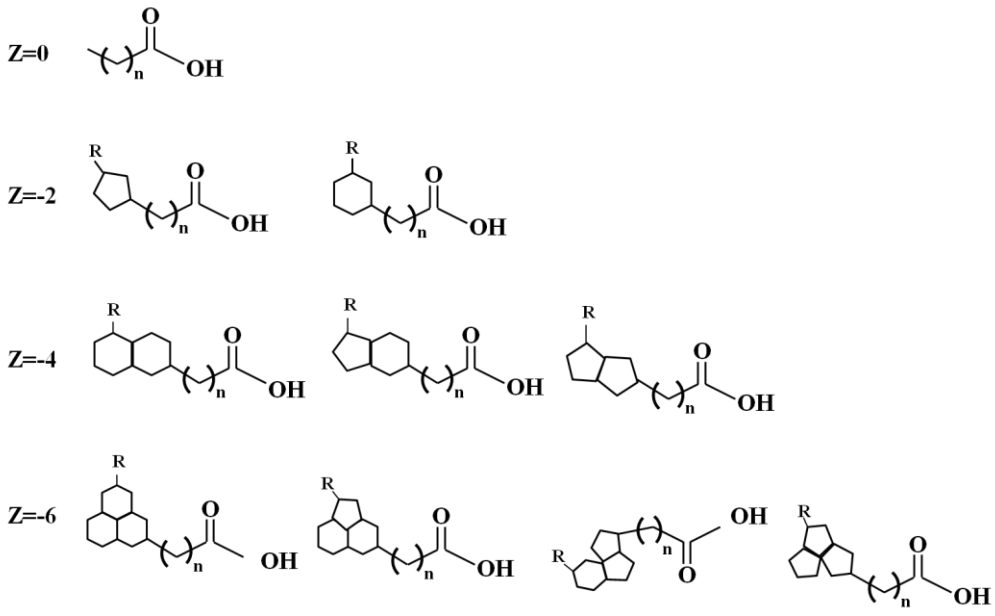

Figure 1-1: Structures of naphthenic acids, where R is an alkyl chain, n is the number of CH2 units.

Since the composition and structure of the NA vary from one crude oil to another, so does the physical and chemical properties. In general, the NA are viscous substances, with a density very close to the one of water. The colour can be pale yellow to dark amber, and have musty hydrocarbon odour. The NA are weak acids, with an acid dissociation (pK) value of almost 5 (Kannel & Gan, 2012). The main mechanism leading to acidity of the heavy and extra heavy crude oils is biodegradation. The mechanism increases the density (lower °API) and synthesizes the naphthenic acids, and the correlation is shown in figure 1-2. The higher the TAN, the lower the API gravity.

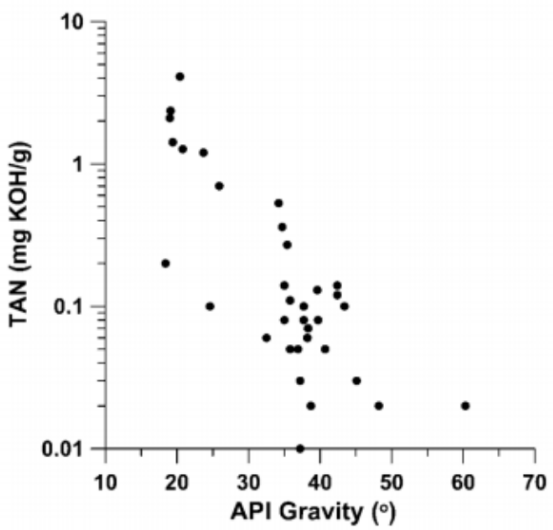

Figure 1-2: Biodegradation increases the density (lower °API) and synthesizes naphthenic acids (Katz & Robison, 2006).

The NA are produced during biodegradation of hydrocarbons in the reservoir (Mackenzie, et al., 1983), and are considered to be a class of biological markers which is linked to the maturity and the extent of biodegradation in the oil fields. The degree of biodegradation increases the TAN by formation of NA.

The NA are amphiphilic molecules, where the hydrocarbon skeleton represents the hydrophobic oil-soluble part. The carboxylic group represents the water-soluble polar head-group (Pathak & Kumar, 1995). Since NA have these properties, the molecules can be distributed in both phases, and even adsorb at the interface. This adsorption has the ability to stabilize colloidal structures, and the NA can be considered as surfactants (Sjöblom, et al., 2003).

The amphiphilic nature of the NA makes them soluble in both water and oil, and being present in both phases of an oil-water system. The distribution is dependent on conditions like the pH and salinity of the aqueous phase and can be described as the equilibrium in equation 1.1:

$$[RCOOH]_O \leftrightarrows [RCOOH]_w \tag{1.1}$$

Where $[RCOOH]_o$ is the concentration of NA in oil, and $[RCOOH]_w$ is the concentration of NA in water. The corresponding partitioning coefficient $K_{w/o}$ is given in equation 1.2:

$$Kw_{/o} = \frac{[RCOOH]_w}{[RCOOH]_O} \tag{1.2}$$

If the NA molecule has a large hydrocarbon part, it is more soluble in the oil phase and the partitioning coefficient shows a lower value than if the molecule had smaller hydrophobic parts. Also, the pH affects the distribution of the NA. If the pH is increased, the carboxylic acids will dissociate and get a negative charge which makes it more water-soluble (Reinsel, et al., 1994).

A pressure drop usually occurs during transportation of the crude oil and water mixtures from reservoir to the topside process facilities. That may cause degassing of the oil. Gases like carbon dioxide are released, which leads to a higher pH in the crude oil and then dissociation of the NA. Stable emulsions will be formed in this case as a result of the dissociated acids affinity towards the interface (Brandal, 2005). The emulsions exhibiting high stability are usually undesirable during the crude oil separation process.

1.2 Metal naphthenates: formation and problems associated with their occurrence

Under certain conditions the NA will form metal naphthenates (MeNA) with metal cations in the co-produced water. Deposition of the metal naphthenates can be troublesome at process facilities, especially when refining heavy crude oils with high TAN (Rousseau, et al., 2001).

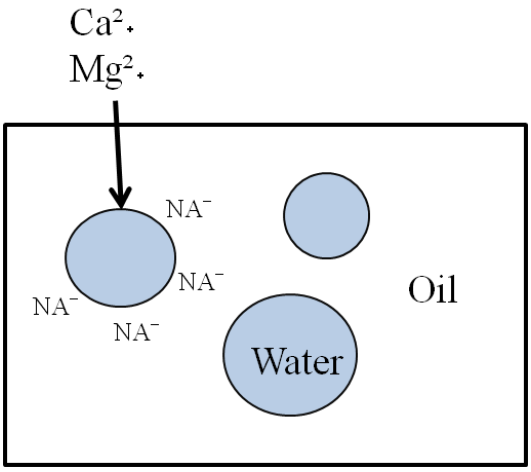

Figure 1-3: Metal cations in co-produced water dispersed in crude oil with NAs, where a reaction occurs at the interface and creates metal naphthenates.

MeNA form when the NA in the crude oil comes in contact with metal cations, like calcium and magnesium, in the co-produced water (figure 1-3). This reaction occurs when the crude oil is transported from the reservoir to the processing facilities.

From reservoir to processing facilities, the pressure decreases, this leads to degassing of carbon dioxide (eq. 1.3). The degassing of gas molecules causes increase of pH and dissociation of NA (eq. 1.4), which facilitates the reaction between NA and calcium (eq. 1.5) (Sheperd, 2008):

$$HCO_3^- + H^+ \leftrightarrow CO_2 + H_2O \quad (1.3)$$

$$R(COOH)_4 + 4OH^- \leftrightarrow R(COO^-)_4 + 4H_2O \quad (1.4)$$

$$R(COO^-)_4 + 2Ca^{2+} \leftrightarrow R(COO)_2Ca \quad (1.5)$$

The NA dissociate at the interface, between the crude oil and the co-produced water. After dissociation, the acids (RCOO-) can react with the metal cations (M^{2+}) in the water, and form naphthenates, as shown in totality in equation 1.6:

$$M^{2+} + 2RCOO^- \underset{k_2}{\overset{k_1}{\leftrightarrow}} [RCOO-M]^+ + RCOO^- \overset{k_2}{\rightarrow} (RCOO)_2 - M \qquad (1.6)$$

The MeNA then start to agglomerate in the oil phase, and accumulate at process unit surfaces (Brandal, 2005). Statoil and ConocoPhillips made a discovery of the ARN molecule in 2004. ARN is a tetrameric acid with four carboxylic acid groups as seen in figure 1-4, with the chemical formula $C_{80}H_{142}O_8$, and a molecular weight of 1231 g/mol.

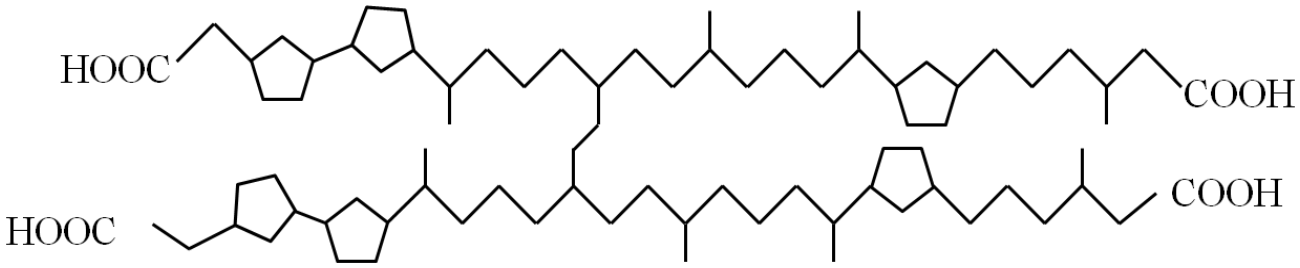

Figure 1-4: The tetrameric naphthenic acid, ARN, which was discovered by Statoil and Conoco Phillips in 2004. ARN has a molecular weight three times higher than the average NA.

The new family of NA has a molecular weight three times higher (1227-1235 g/mol) than the average mole weight of NA found in crude oil (430 g/mol) (Statoil, 2007). The 4-protic carboxylic acids contain 4-8 unsaturated sites/rings in the hydrocarbon skeleton (Baugh, et al., 2005). The ARN molecule can form large networks if in contact with Ca^{2+}, and is a big contributor to the MeNA depositions.

The MeNA is a sticky, solid deposit which precipitates in the process facilities, since is not soluble in water nor oil. The density of the MeNA is lower than water and higher than oil, which makes it accumulate in the oil/water interface in separators and de-salters, but can also deposit in tubes and pipelines (Havre, 2002). The precipitation can reduce the production flow, and hardens on contact with air. This formation must be cleaned, and can lead to costly shutdown periods.

Figure 1-5: Metal naphthenate deposits in flash drum (left) (Mediaas, et al., 2007), and in hydrocyclone (right) (Scaled solutions LTD, 2014).

Since 1995, Statoil has been production operator at the Heidrun field, and the crude oil is characterized by a high TAN and relatively low density (0,90 g/cm^3). The Heidrun field experienced problems with naphthenate already in September 1996, and recognised in 1997 that it would be a constant threat against flow assurance. The calcium naphthenate (CaNA) clogged jet nozzles, jet water outlets, instrument outtakes and separator internals (figure 1-5). Sand was held up by the sticky naphthenate at the interface in the separators, and led to large lumps falling to the bottom (Vindstad, et al., 2003). The deposition of CaNA led to increased maintenance costs and reduced operational regularity.

Problems with CaNA in Nigerian oil fields were reported by SPE international symposium on oilfield chemistry in 2013. Before the CaNA was identified, the operating expenses and man-hours were increased to manually remove the solids which had deposited. Over a six-week vessel cleaning operation, where precipitated solids were transported from the facilities, approximately 30 tons of solids were sent onshore. Vessel cleaning during the facility shut-down alone was estimated to cost USD 6 million (Igwebueze, et al., 2013).

The higher the pH, the more dissociated the NA will become, and the more likely it becomes that the NA will react with metal cations at the interface. The use of acid is the most traditional way to inhibit the formation of metal naphthenates, but is a fairly expensive procedure which increases corrosion and is not good for the environment. When adding acid to the crude oil, the pH drops causing a decline in the dissociation of the NA to the anionic functional groups. This leads to the growing surface tension, and the stabilizing ability of the NA goes down (Rodriguez & Ubbels, 2007). The added acid should have a pK_a lower than the NA, and lead to a pH around 6.0. If the pH is lowered even more, it could cause corrosion problems. (Kelland, 2009).

The most common acids currently used by industry for the metal naphthenate inhibition are (Ubbels, 2004):

- Phosphoric acid (inorganic mineral acids)
- Acetic acid or glycolic acid (small organic acids)
- DDBSA – Dodecylbenzenesulfonic acid (surfactant acids)

Another option is to use specialty surfactants known as naphthenate inhibitors. To inhibit naphthenate salt formation, the surfactants crowd the interfacial surface between oil and water, as seen in figure 1-6. Since the surfactant is more interfacially active, it makes no room for the NA, and lowers the probability of MeNA formation (Rodriguez & Ubbels, 2007).

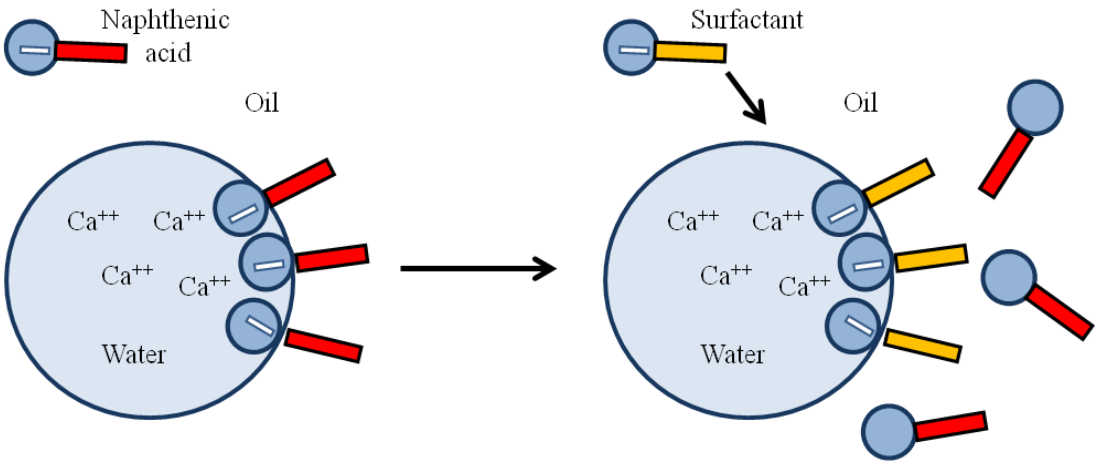

Figure 1-6: Specialty surfactants (yellow) known as naphthenate inhibitors use the mechanism of interfacial crowding to inhibit salt formation between naphthenic acids (red) and calcium.

1.3 Methods of naphthenic acid removal

The formation of metal naphthenates can be inhibited, but methods to remove naphthenic acids before they react with metal cations are of greater interest. Methods currently used in the industry include dilution of a crude oil with high TAN by a crude oil with low TAN, which is not favourable because of the decrease in quality and value of the low TAN crude oil. Also, caustic washing has been used frequently, but is not good for the environment and wastes oil (Huang, et al., 2005). The method creates large amounts of wastewater, and generates emulsions which are difficult to treat.

Non-destructive methods like solvent extraction (Duncum & Osborne, 2002) and adsorption (Gillespie & Arena, 1995) does not completely remove the NA. Another method is hydrotreating with cobalt, molybdenum or nickel oxides supported on alumina (Halbert, et al., 1999), which is a successful method, but requires the use of hydrogen gas. Several newer methods for NA removal have appeared, due to increasing demand of heavy crude oil with high TAN. Here are some of the methods listed:

Amino acid ionic liquids

Several uses of amino acid ionic liquids (AAILs) have been reported, for instance extraction of sulphur (Collins, et al., 2007), sequestration of CO_2 from petroleum fractions (Bates, et al., 2002) and separation of CO_2 (Zhang, et al., 2006). Anderson et al. reported the use of AAILs for removal of NA, through the formation of a zwitterionic complex. The method was shown to be successful in the neutralization and extraction of naphthenic acids from crude oil. The

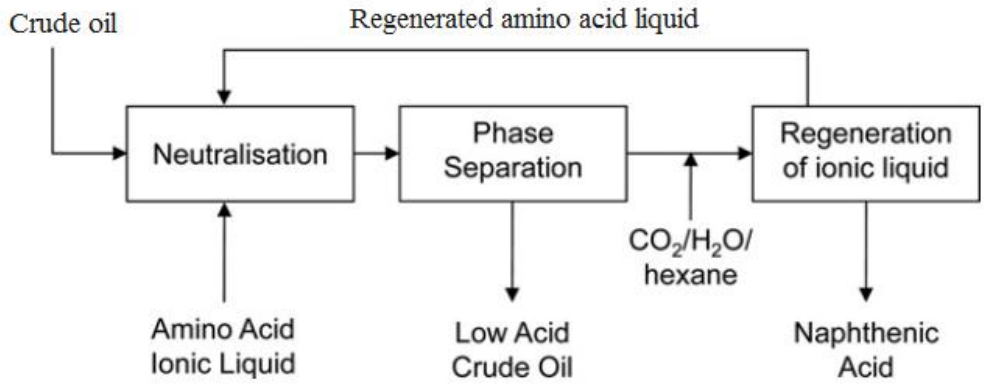

Figure 1-7: Graphical abstract of the removal of NA using amino acid ionic liquids (Anderson, et al., 2013).

reaction occurs between one amino group of the amino acid-anion and one carboxylic acid group, which forms a zwitterionic complex. The complex can be reacted with carbonic acid to reform the ionic liquid (Anderson, et al., 2013). The process is illustrated in figure 1-7.

Catalytic decarboxylation on magnesium oxide

Zhang et al. have studied the use of the metal oxide catalyst, MgO, for removal of NA by catalytic decarboxylation on magnesium oxide. The catalyst has several functions, like adsorption of acidic compounds by acid-base neutralization, and contributes to decarboxylation and hydrocarbon cracking (Zhang, et al., 2005). As illustrated in figure 1-8, a flow reaction line was tested for crude oil samples by Zhang et al. A HPLC pump was used to pump decane, which again pushed out crude oil to a stainless steel reactor. The catalysts were placed in the stainless steel reactor. The amount of produced CO_2 during reaction, and the acid conversion were parameters used to assess if the NA removal was successful.

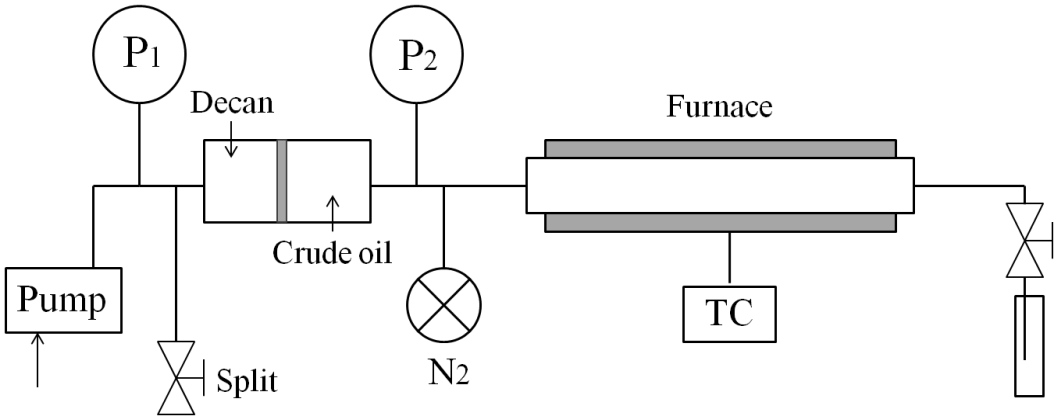

Figure 1-8: Schematic of fixed-bed flow reaction system.

Catalytic decarboxylation with MgO was determined to be successful, but still requires moderately high operating temperatures up to 250 °C. The process leads to decreasing of TAN and the removal of NA. Zhang et al. reported that the reaction mechanism could be complex, and may involve a series of reactions, such as acid-base neutralization, oxidative decarboxylation and ketonization of carboxylic acids.

Ammonia solution of ethylene glycol

The extraction of NA by using an ammonia solution of ethylene glycol was reported by Wang et al. The second vacuum fraction (SVF – vacuum gas oil pumped from the second position in the vacuum distillation tower) and the ammonia solution of ethylene glycol were mixed in a three-neck flask, with constant stirring at 10 minutes and temperature of 50-60 °C. The mixture was added to a separation funnel for 1 hour at 70 °C after the extraction, so gravity could separate the solution with extracted NA from the oil (figure 1-9).

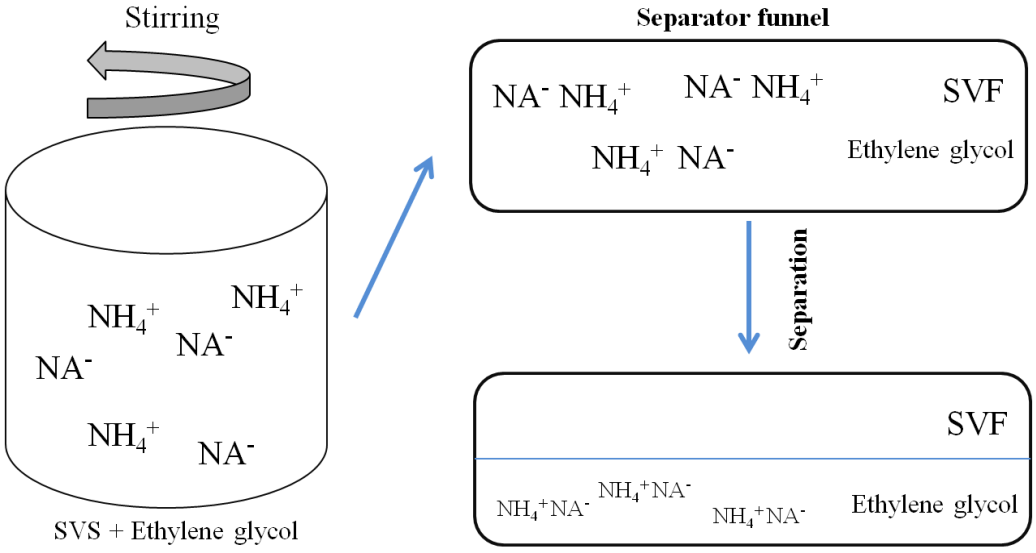

Figure 1-9: SVF with NA mixed with ammonia solution in ethylene glycol gets stirred, sent to separator funnel, and separated.

Since the phase with naphthenic ammonia salt was in the bottom phase of the funnel, that part was heated to 120 – 150 °C. The heating leads to decomposition of the salt into NA and ammonia which evaporates. Then the NA can be isolated and used for other useful purposes (Shi, et al., 2002).

The method is successful in NA removal, but requires a large excess of organic base to achieve good extraction. This can lead to a carryover of amine into the oil phase, and can be problematic for the downstream catalyst (Laredo, et al., 2003).

Catalytic esterification with methanol

Wang et al. introduced a process for NA removal, which is based on the treatment of NA with methanol under conditions sufficient to form naphthenic acid esters. This esterification was catalysed by a solid Lewis acid, SnO, which increased the acid removal ratio. The TAN was lowered by the conversion of NA to methyl naphthenate.

The experiment was executed in an autoclave, with constant stirring and nitrogen atmosphere. Optimal reaction temperature was 300 °C, suitable amount of methanol was 5.0 wt % and for the SnO catalyst it was 4.0 wt %. Also, the amount of acid removal increased with increasing reaction time. The acid removal with SnO in 1 hour was equal to the acid removal without SnO in 6 hours (Wang, et al., 2008).

Successful removal of NA, but requires filtering and high temperatures up to 300 °C over prolonged time. Also, the use of methanol is not favourable for the environment.

2. Magnetic nanoparticles

Magnetic nanoparticles (MNP) are increasing in interest for researchers in several disciplines, like data storage (Hyeon, 2003), catalysis (Tsang, et al., 2004) and biotechnology (Gupta & Gupta, 2005). New areas of use are increasing for the MNP, and represent high potential for the removal of NA.

2.1 Materials and synthesis

There are a number of different compositions and phases that MNP can be synthesized from, like iron oxides such as Fe_3O_4 and γ-Fe_2O_3 (Neveu, et al., 2002), pure metals such as Fe and Co (Puntes, et al., 2001), spinel-type ferromagnets, such as $MgFe_2O_4$, $MnFe_2O_4$ and $CoFe_2O_4$ (Park, et al., 2004), as well as alloys, such as $CoPt_3$ and FePt (Sun, et al., 2000). The synthetic route to shape-controlled, highly stable and monodisperse MNP has been evolving to be efficient the last few years. Some of the common methods for synthesizing the MNP are described below.

2.1.1 Co-precipitation

The method called co-precipitation is a simple way to synthesize iron oxides (Fe_3O_4 or γ-Fe_2O_3), and uses aqueous salt solutions of Fe^{2+}/Fe^{3+} (Willis, et al., 2005) as illustrated in figure 2-1. Base is added under inert atmosphere at room temperature or a bit higher (20-90 °C). The shape control is not the best, and the size distribution is somewhat narrow. On the other hand, the reaction time is only minutes, and is considered to be the simplest method (Schüth, et al., 2007).

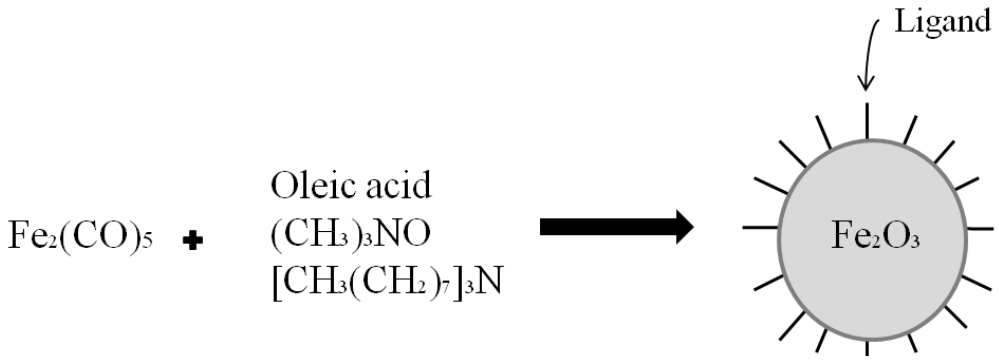

Figure 2-1: Preparation of γ-Fe_2O_3 nanocrystals by co-precipitation.

2.1.2 Thermal decomposition

Initially, the thermal decomposition reaction leads to a metal if the precursor contains a zerovalent metal, such as in carbonyls. If a two-step procedure is used, the reaction can lead to oxide nanoparticles (Hyeon, et al., 2001) as shown in figure 2-2.

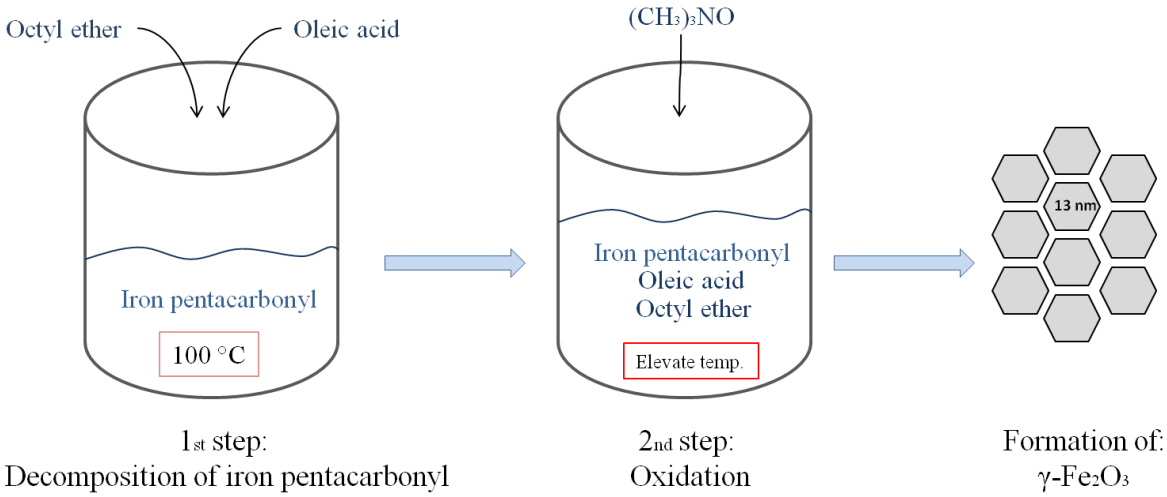

Figure 2-2: An example of formation of γ- Fe_2O_3 nanoparticles at approximately 13 nm by thermal decomposition with a two-step procedure.

The thermal decomposition is a complicated method for synthesizing MNP, which requires high temperatures up to 320 °C. The reaction period can take hours or days, and occurs in an organic compound. The size distribution is narrow, and the yield is high. The method is considered to be the best in size and morphology control. The important parameters for size and morphology control are the ratios of the starting reagents: organometallic compounds, surfactant and solvent. For precise control, the reaction temperature, reaction time and aging period may also be decisive.

MNP were prepared by thermal decomposition of $Fe(CO)_5$, by the presence of polyisobutene in decalin under nitrogen atmosphere at 170 °C. These particles can be made quite monodisperse, and the size can be tuned by varying the $Fe(CO)_5$/polymer ratio (Butter, et al., 2002).

2.1.3 Microemulsion

A microemulsion is not a kinetically stable dispersion as an emulsion, but it is a thermodynamically stable dispersion of to immiscible liquids. The dispersion is stabilized by surfactant molecules. In w/o emulsions, reverse micelles are formed around the dispersed water droplets (figure 2-3), which typically have a diameter of 1-50 nm.

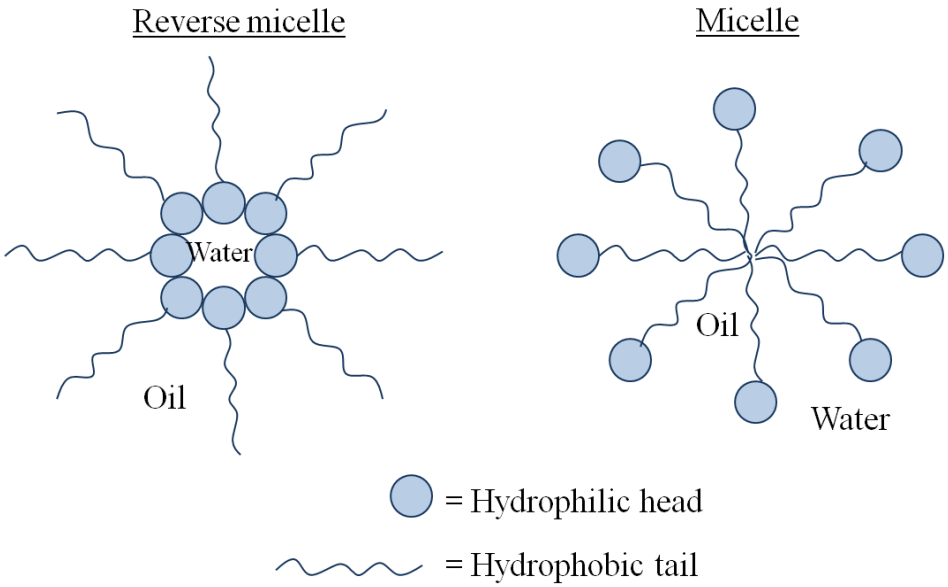

Figure 2-3: The surfactants can form aggregates, where the hydrophobic tail is turned outwards in continuous oil phase (reverse micelle) and the hydrophilic head is turned outwards in continuous water phase (micelle).

In w/o microemulsion, water is dispersed in oil as microdroplets, surrounded by a monolayer of surfactants. Soluble metal salts can be included inside the droplets, which will continuously collide, coalesce and break again (Lawrence & Rees, 2000), as illustrated in figure 2-4. The microemulsion is a complicated method, which is executed at ambient conditions and the reaction time is a couple of hours. The reaction requires large amounts of organic solvent, and the yield is low. Although magnetic nanoparticles have been produced with this method in a controlled manner, the particle size and shape vary over a wide range. The process is less efficient than thermal decomposition and co-precipitation, and difficult to scale-up.

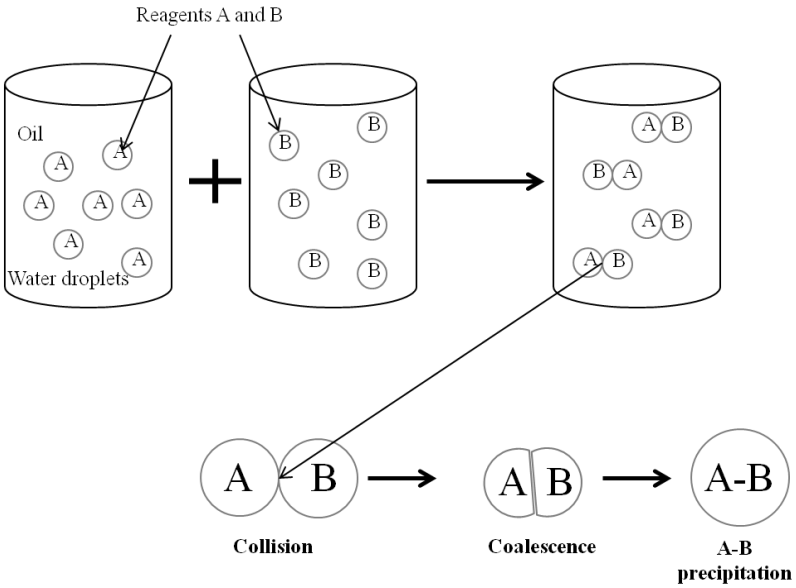

Figure 2-4: Two different w/o microemulsions, respectively with reagent A and B, mixed together so the droplets can collide, coalesce and form A-B precipitate.

2.1.4 Hydrothermal synthesis

A little explored method for the MNP generation is hydrothermal synthesis, known for producing high-quality nanoparticles. It is a simple method, which requires high pressure and high reaction temperatures up to 220 °C, and the reaction time is hours to days. Wang et al. reported a generalized hydrothermal method for synthesizing several different kinds of nanocrystals by liquid-solid-solution reaction (LSS). The solid is represented by metal linoleate, the liquid phase is ethanol-linoleic acid and the solution is a mixture of water and ethanol. The method is based on a general phase transfer and separation mechanism which occurs at the interfaces between liquid, solid and solution (Wang, et al., 2005).

2.2 Protection and stabilization

Particles in the nanometer size range have intrinsic instability, which can lead to agglomeration. Therefore, the MNP must be stabilized before applying them in a process, because the naked MNP are chemically highly active. Pure metals, like Fe, Co, Ni and their metal alloys, are especially sensitive to air. The receptivity towards oxidation also increases with decreasing size of the particles, and thus making it important to protect the nanoparticles. Lack of protection can lead to loss of magnetism and dispersibility (Xie, et al., 2013).

All described protection strategies rely on a core-shell structure, where the MNP are the naked cores, and a shell surrounding them for protection against the environment. The MNP can be oxidized by oxygen, or eroded by acid or base. The coating strategies can be divided into two major groups:

- Coating with organic shells (Sahoo, et al., 2001), including surfactant (Euliss, et al., 2003) and polymers (Liu, et al., 2004).

- Coating with inorganic components, including silica (Kobayashi, et al., 2003), carbon (Lu, et al., 2005), precious metals (Sobal, et al., 2002) and oxides (Nunez, et al., 2004).

The naked MNP can also be dispersed in a matrix, often made up of a polymer, silica or carbon. This reduces agglomeration and oxidation, but they are then stuck in a fixed media. The method of individually protected MNP is preferred, and keeps the particles freely dispersed (Kim, et al., 2003).

2.3 Functionalization

A coating on the MNP gives protection against the environment, but can also be used to functionalize the surface with functional groups. The magnetic core, also referred to as the naked MNP, can be coated with a protecting shell which is then functionalized with molecules of desired properties. Since the NA have carboxylic acids groups, it would be interesting to look further into functionalization with amino groups. The functionalized magnetic nanoparticles are often referred to as FMN.

2.3.1 Grafting with amino-functional alkoxysilanes on silica

The MNP can be modified with alkoxysilanes via silylation reaction, where the reagents commonly used contain non-hydrolyzable amino groups. The most common alkoxysilane used for functionalization is 3-amino-propyl-triethoxysilane (APTES), because of its terminal

amino group. FMN grafted with silica and alkoxysilanes promotes hydrophilic properties, but the large diversity of alkoxysilanes generates several possibilities for nanoparticle surface functionalization. Bini et. al. used iron oxide nanoparticles to find that 3-aminopropyl-ethyl diethoxy-silane (APDES) and 3-aminopropyl-diethyl-ethoxysilane (APES) convey greater stability than APTES, which has a larger surface potential. APDES has the insertion of an ethyl group and APES has two ethyl groups, and both have smaller amino group densities and zeta potentials. The higher colloidal stability of APDES and APES are a consequence of the steric contributions given by the ethyl groups (Bini, et al., 2011). The FMN with the different amino-functionalized alkoxysilanes are illustrated in figure 2-5.

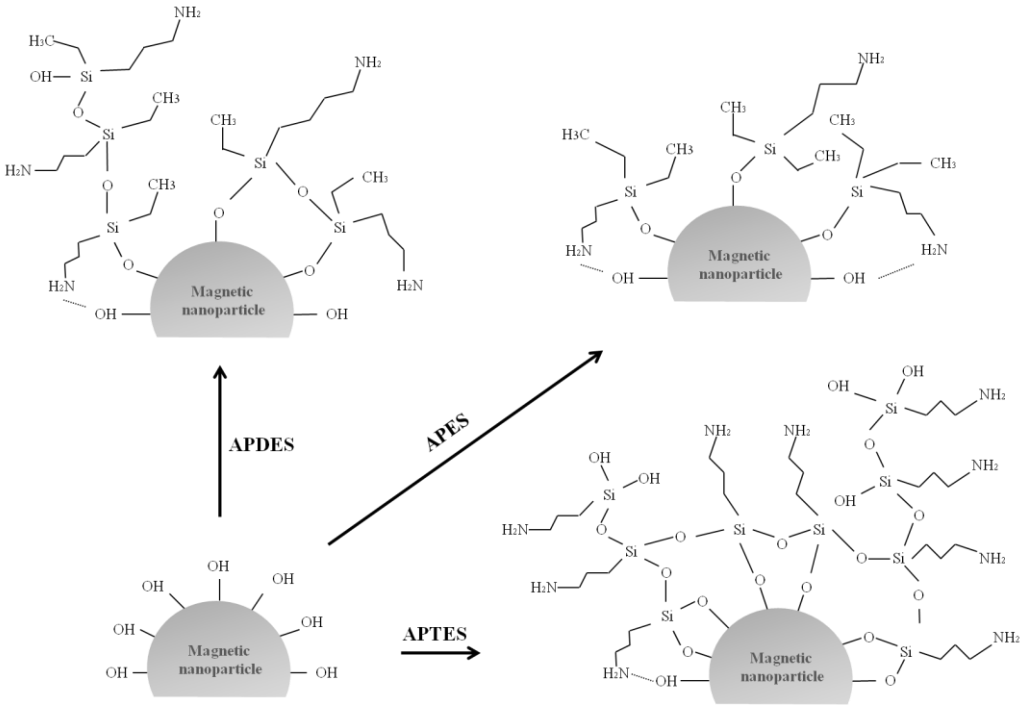

Figure 2-5: Magnetic nanoparticle functionalized to 3-aminopropyl-diethyl-ethoxysilane (APES), 3-aminopropyl-ethyl-diethoxy-silane (APDES) and 3-amino-propyl-triethoxysilane (APTES).

2.3.2 Silica with mixed functional ligands

Zhang et al. reported the synthesis of silica coated MNP that have the ability to be functionalized by mixed ligands, with different functional groups. This property enables the surface of the FMN to attract targets with different functional groups. The silica coating was functionalized with both C_{18} and NH_2. The MNP of Fe_3O_4 were coated with silica by the addition of tetraethyl orthosilicate (TEOS) after synthesis of the naked magnet core.

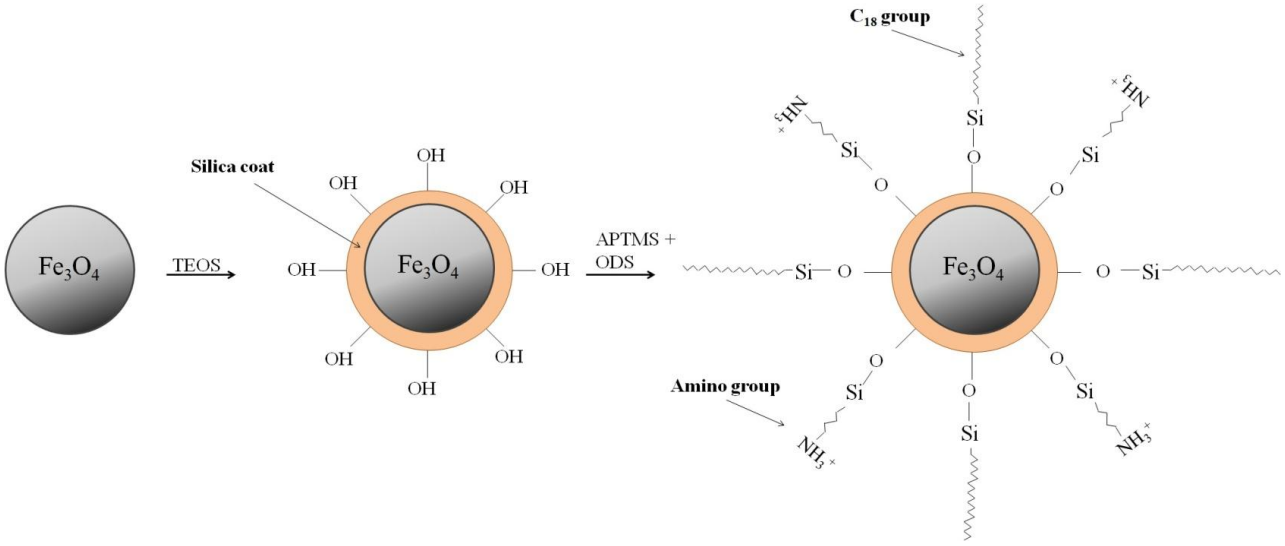

Figure 2-6: The functionalization of MNP (Fe_3O_4) with silica modified by C_{18} and amino groups.

Then the silica was functionalized by octadecyltriethoxysilane (ODS) and aminopropyltrimethoxysilane (APTMS), so the functional groups C_{18} and NH_2 could be attached to the surface, as illustrated in figure 2-6.

The functionalization method was successful in the removal of anionic organic pollutants in acidic conditions, and indicated high extraction performance. The functional groups were said to provide hydrophobic interaction and electrostatic attraction (Zhang, et al., 2011).

2.3.3 Possible application of functionalized magnetic nanoparticles for naphthenic acid removal

The performance of magnetic nanoparticles depends on the type of material and size, which is typically 10-20 nm. A number of materials can be used for the synthesis, including iron oxides Fe_3O_4, pure metals Fe and Co, spinel type ferromagnets $MgFe_2O_4$, $MnFe_2O_4$, or $CoFe_2O_4$ (Schüth, et al., 2007).

Chemical stabilization of these particles is usually required as they are easily oxidized in air, resulting in loss if magnetic properties and reduction of dispersibility. In many cases the stabilization strategies, such as surface coatings with polymers, surfactants, or inorganic compounds, not only protect the particles, but can also be used for further functionalization

(Xie, et al., 2013). Amino groups are capable to attract NA, by interaction of the lone pair of electrons on the nitrogen with the carboxylic acid on NA.

One of the possible options would be coating Fe_3O_4 nanoparticles with a thin layer of silica (sol-gel technique) to make the surface amenable for further amino-functionalization. Chelation agents, such as bidentates, exhibiting a high affinity for metal ions, and capable of creating bonds with two different atoms, will be used to enhance the amino-functionalization. Other methods based on brush polymers and specialty polymers can also be considered.

The use of silica as a protection for the magnetic core of the MNP is widely used, and also makes it easy to functionalize the surface. Another possibility is also to coat the Fe_3O_4 nanoparticles with silica, but to functionalize the surface with mixed ligands, like C_{18} and NH_2. Since the NA are amphiphilic molecules, there is a possibility that the mix of hydrophilic and hydrophobic ligands could attract NA.

The silica coating can also be functionalized by amino-functional alkoxysilanes, which is a large group of molecules. They vary in amino group densities and colloidal stability, depending on the molecular structure. This presents many options for functionalization.

The dual nature of the FMN could also be accomplished by the use of polymers, like Zhang et al. did in 2010. The naked MNP were covered in hydrophobic C_{18}, but the hydrophilic polymer chitosan-tripolyphosphate was added to the surface, which was also claimed to increase the dispersibility of the nanoparticles.

3. Magnetic phenomena

A magnet is a material that generates a magnetic field, like the common bar magnet which is illustrated in figure 3-1. Magnets have a south and a north pole, and the opposite poles attract each other while the alike repel each other. Magnets have the property of a force that draws on other ferromagnetic materials. These materials, such as iron, nickel and cobalt, are attracted to the magnetic field of a magnet, and can also be magnetized (Macintyre, 1999).

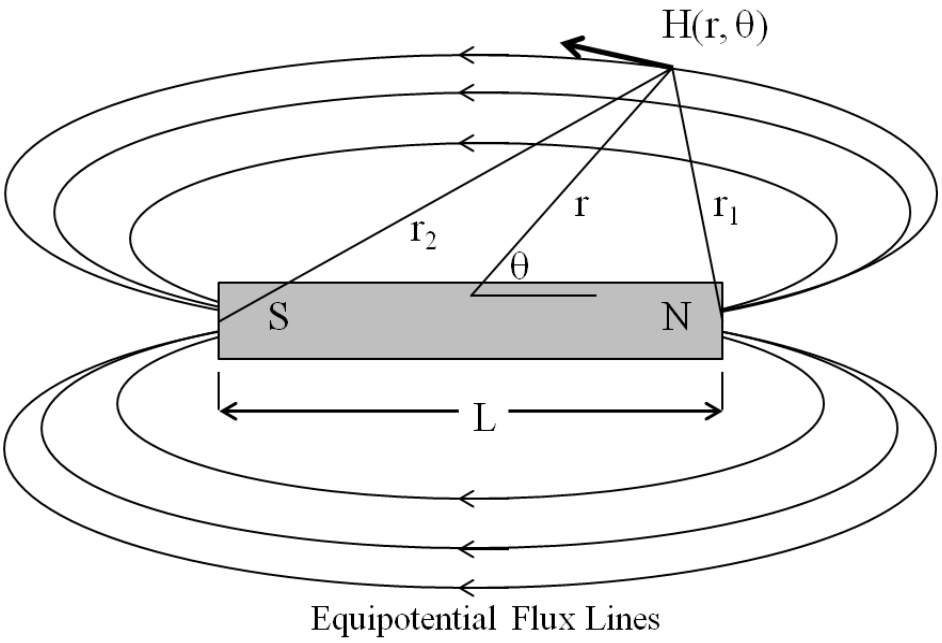

Figure 3-1: Magnets produce magnetic fields, illustrated as a bar magnet.

A magnetic field is a vector quantity which has both magnitude (strength) and direction properties, and is created by the electron spins inside the magnet. It is an electrostatic field moving in a very high speed. The magnitude of a magnetic field is determined by the effect it has on a moving charge. A force is produced by the magnetic field, and can be detected. The magnetic field is produced when an electrical charge is in motion, like an electrical current flowing in a conductor or permanent magnet (Jiles, 1998). Magnetic fields are also produced by electric currents, as illustrated in figure 3-2.

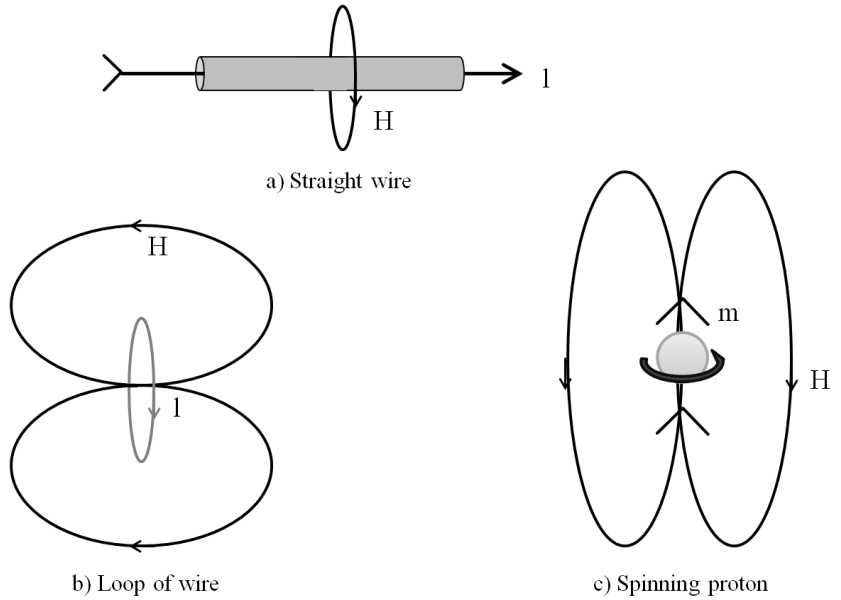

Figure 3-2: Magnetic fields can also be produced by electric currents: through a straight wire (a), a loop wire (b) or a solenoid (c).

The magnetic field, H, produced by a magnetized object is defined as in equation 3.1:

$$\vec{H} = \frac{3(\vec{m}\times\hat{a}_r)\hat{a}_r - \vec{m}}{r^3} \tag{3.1}$$

Where $\hat{a}_r$ is a vector unit along r, and r is the distance between the magnetic field source and the measurement point. Like magnetic fields, magnetization is a vector quantity and is a material property that can occur from internal magnetic sources as well as induced by an external magnetic field. Magnetization, M, is the intensity or strength of a magnetized object, which depends on the density of its volume-distributed moments (m) (Macintyre, 1999), and is defined as in equation 3.2:

$$\vec{M} = \frac{\vec{m}}{volume} \tag{3.2}$$

The magnetization vector can consist of permanent magnetization components, which does not depend on an external field, and it can consist of induced magnetization components. The

induced magnetization vector depends on an external magnetic field, and only exists while the induced field is present (Macintyre, 1999). Magnetic materials can be classified as:

- Magnetically soft: Magnetization is mostly induced
- Magnetically hard: Permanent magnetization vector dominates, for example: a magnet.

3.1 Magnetic properties of nanoparticles

The behaviour of a magnet changes when the dimensions are lowered to nanometres, and in applications like biomedicine, magnetic fluids and catalysis, the nanoparticles perform their best when the size is below a critical value. The size depend on the material, but usually is around 10-20 nm. Each nanoparticle then consists of a single magnetic domain, which means that the magnetization does not vary across the magnet (Schüth, et al., 2007). When the size of a magnetic particle gets close to the domain wall size, it might be more energetically favourable for the particle to form a single domain (Engen, 2013). The particle is uniformly magnetized with all spins aligned in the same direction, as shown in figure 3-3 (A). This leads to a superparamagnetic behaviour if it is kept over the blocking temperature. The superparamagnetic properties give the magnetic nanoparticles a large constant magnetic moment, and make them fast to response to applied magnetic field (Schüth, et al., 2007). When an external magnetic field is applied, the spins of the single domain particle rotate simultaneously to become parallel to the field. When the field is removed, the MNP retain no residual magnetism. Because of this property, the particles can easily be removed after adsorbing unwanted molecules from the solution, just by applying an external field. It requires no filtration and no centrifugation (Xie, et al., 2013).

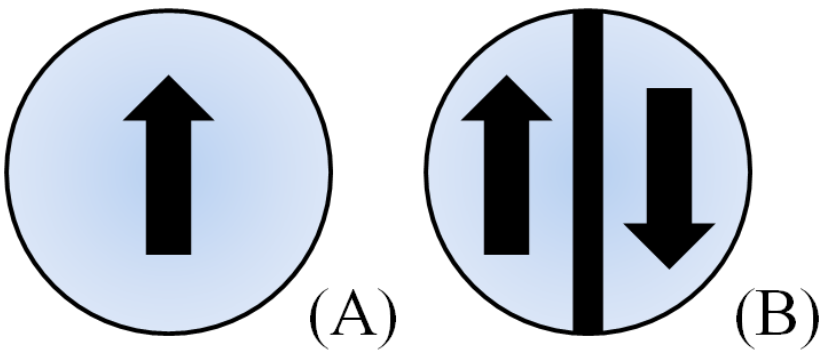

Figure 3-3: Magnetisation of a single domain particle (A), and the simplest multi-domain particle (B).

3.2 Measuring magnetic fields

There are a couple of ways of using units when measuring magnetic fields: The Gaussian cgs (centimetre, gram and second) has been frequently used, but the International System of Units (SI) has become more common with the use of meter, kilogram, second and ampere as the fundamental units (Payne, 1981). The strength of a magnetic field is measured in several different ways by magnetic field sensors, where the different types are illustrated in figure 3-4. First, the sensors are divided into sensors that measures low fields (<1mT) which are called magnetometers. Sensors that measures high fields (>1mT) are called gaussmeters.

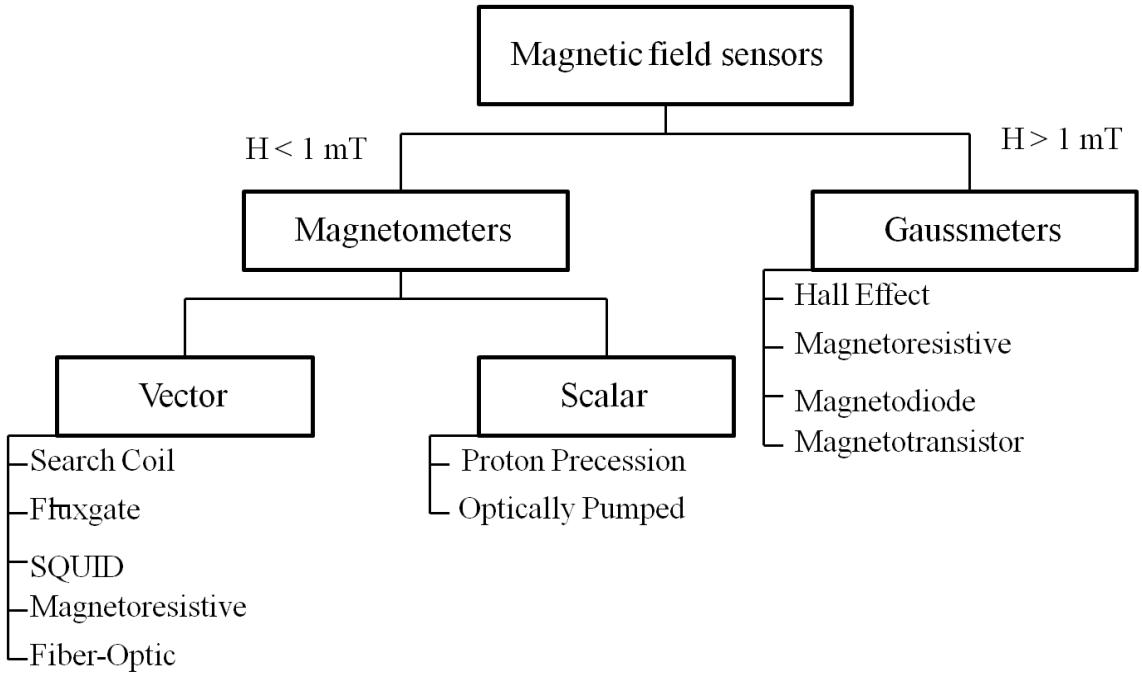

Figure 3-4: Magnetic field sensors are divided into two categories: magnetometers for low fields, and gaussmeters for high fields.

4. Interfacial processes

Adsorption of NA to FMN is crucial for the removal of NA from the crude oil, and is a phenomenon which describes the binding of a molecule/atom/particle to the surface of a liquid or solid surface. The substance which is adsorbed to the surface is called the adsorbate, and the substance of which it is adsorbed is called adsorbent (Keller & Staudt, 2006). Adsorption is divided into physical (physisorption) and chemisorption, and some differences are described in table 4.1:

Table 4.1: The differences between the two types of adsorption: Physical and chemisorption.

	Physical	**Chemisorption**
Bonds	Weak Van der Waals forces, intermolecular forces	Strong chemical bonding
Heat of adsorption	Low, about 4-60 kJ/mol (equivalent to heat of condensation)	High, about 40-400 kJ/mol (equivalent to chemical reactions)
Specificity	Unspecified	Specific on certain sites
Electron transfer	No	Yes, leading to bond formation
Reversible process	Yes	No
Activation energy	No	Yes, small
Molecular layers	Multilayer	Monolayer

Physisorption

The term physisorption corresponds to the weakest bonding between adsorbate and adsorbent, namely Van der Waals forces. The heat of adsorption is low (about 4-60 kJ/mol), and there is no activation energy. This physical adsorption makes it possible to determine the total surface area of particles. The other type of adsorption is chemisorption, and is compared with physisorption in figure 4-1 on the basis of potential energy and distance to surface. Chemisorption is further described in the section below.

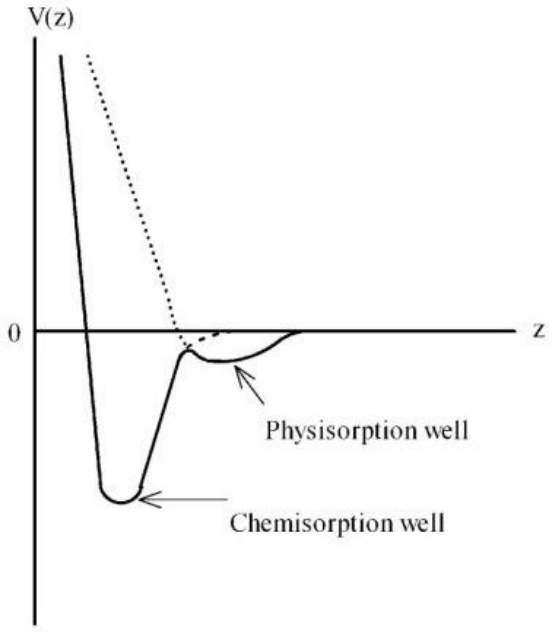

Figure 4-1: Potential energy curve for chemisorption (dashed line) and physisorption (dotted line) (Wilks, 2010).

Chemisorption

The term chemisorption correlates to the case of strong chemical bonding between adsorbate and adsorbent. The heat of adsorption is high (about 40-400 kJ/mol), and there is a small activation energy. The strong interaction causes a change in the chemical state of the adsorbate. Chemisorption of molecules can cause dissociation, and lead to formation of new molecules, as illustrated in figure 4-2.

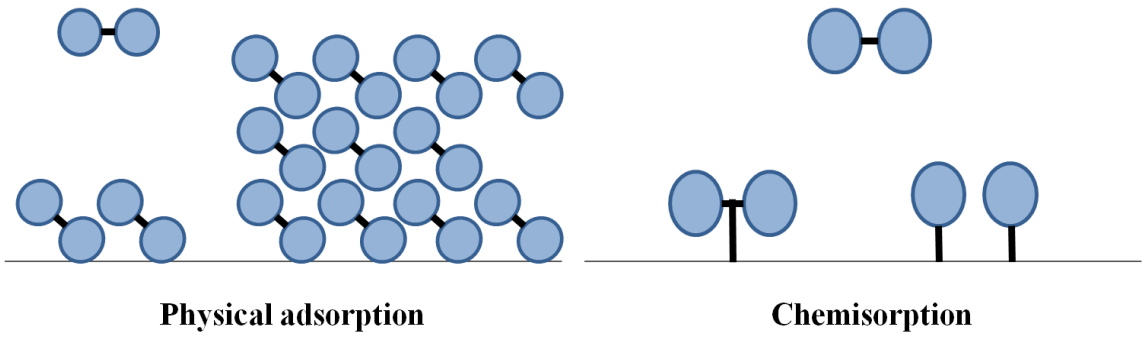

Figure 4-2: Two kinds of adsorption; Physical adsorption forms multilayers, and chemisorption forms monolayers. The chemisorption can be associative or dissociative.

4.1 Adsorption kinetics

The adsorption of NA from an organic solution by the functionalized nanoparticles can be described by three consecutive steps:

1. Film diffusion. This is a transport of the NA from the bulk solution to the outer surface of the particle by the molecular diffusion. There is no actual film surrounding the particle, it just describes the resistance of the mass transfer at the surface of the particle. The mass transfer coefficient, K_f, in film theory, is related to the free liquid diffusivity of the solute, D_e, and the thickness of the diffusional sublayer, δ as follows:

   $$K_f = \frac{De}{\delta} \quad (4.1)$$

   The driving force in film diffusion is the concentration gradient in the liquid film around the particle.

2. Internal diffusion. This involves the transport of NA from the particle surface into interior sites by diffusion within the liquid-filled pore and migration along the solid surface of the pore (surface diffusion). Both processes will act at the same time and the faster one will control the rate of transport.

3. Adsorption. Occurs when the NA adsorb on the active sites of the surface pores interior. This step doesn't influence the overall kinetics and is very fast.

The overall rate of adsorption will, therefore, be controlled by the slowest step, 1 or 2.

Factors affecting the adsorption

The following features are critical for the adsorption from solution to solid surface:

- The interaction between surface and adsorbed solute
- The structure of adsorbed layer
- The overall process of adsorption is exothermic, which means that the rate of adsorption will decrease with the increase in temperature.

- The chemistry of the solid surface is important for adsorption. Even for the more similar materials, the surface can vary because of contamination or difference in preparative methods. Silica is a material which can be porous or non-porous, and the hydroxyl groups can vary in type and number based on the preparation method and how it is treated before experiments (Ganichenko, et al., 1959).

- The solute and its interaction with the solvent is also significant, and is influenced by the solutes chain length, physical state in solution, nature of polar groups and ring structure, which again influence the solubility. In general, a solute will be less adsorbed with increasing solubility in the solvent, hence, the solute will be more strongly adsorbed with decreasing solubility. This is given that the specific interactions with the surface do not dominate (Parfitt & Rochester, 1983). A correlation between adsorption and chain length has been accepted a while, and Traube's early experiments on the subject led to Traube's rule (Traube, 1891). He investigated the liquid-vapour interfacial tension (γ_{lv}) of hydrocarbon acid, alcohol, ester and ketone homologues dissolved in water. Traube observed a pattern of which the molar concentration necessary to reduce γ_{lv} to a chosen value decreased in regular progression with every added methylene unit within a specific homologous series (Krishnan, et al., 2003). The rule, however, applies only with high dilution, and is not true in the situation of adsorption at the solid/liquid interface. A quantitative relationship does not exist, but qualitative trends are of interest. The number of aromatic rings will also influence the adsorption, as demonstrated by Kiselev and Shikalova (Kiselev & Shikalova, 1970). Solutes can also be associated in the solution, for example the formation of micelles or the dimeric form of fatty acids in organic media. The configuration of the fatty acids in the adsorbed layer relies on the relative strength of their interaction with the surface and of the association (Parfitt & Rochester, 1983).

- The solvent can influence the adsorption in three situations: solute in solution, adsorbed solute and the adsorbent. Also, the solvent itself is adsorbed, which is frequent for binary liquid mixtures and not dilute solutions.

4.2 Adsorption equilibria

The equilibrium relationship between adsorbate in solution and adsorbate adsorbed to an adsorbent is described by adsorption isotherms. An equilibrium will be established if the adsorbent and adsorbate are contacted long enough. The experimental measurement for adsorption from solution at the solid/liquid interface is the change in concentration of the solution which results from adsorption at a given temperature (Parfitt & Rochester, 1983).

The adsorption isotherm can be described by a curve, which relates the equilibrium concentration of a solute on the surface of an adsorbent, q_e, to the concentration of the solute in the liquid, C_e, with which it is in contact. The equation below illustrates the q_e and C_e relationship at equilibrium (eq. 4.2) (Wang, et al., 2010):

$$q_e = \frac{C_o - C_e}{C_{solid}} = \frac{(C_o - C_e) \cdot V}{m} = \frac{mass}{mass} \quad (4.2)$$

Where C_o is the initial concentration of adsorbate, C_{solid} is the concentration of adsorbent, m is the mass of adsorbent and V is the total volume. The adsorption equilibrium can be predicted by several models, and some of them are illustrated in figure 4.3.

Langmuir isotherm

The Langmuir isotherm is a equilibrium model which assumes that the adsorbed layer will form as a monolayer, e.g. a single layer of molecules. The model is also based on the assumption that all sites on the surface are equally probable as an adsorption site. The adsorbed molecules are assumed to not move on the surface, but can be lost back to the solution. The Langmuir model is viewed as a dynamic process, where the number of molecules being adsorbed is equal to the number of molecules leaving the adsorbed state at equilibrium. The Langmuir isotherm can be described as in equation 4.3:

$$q = \frac{q_m K_A C}{1 + K_A C} \quad (4.3)$$

Where q_m is the maximum absorbable value of q, and K_A is equal to the adsorption rate constant divided by the desorption rate constant ($K_A = k_1/k_2$).

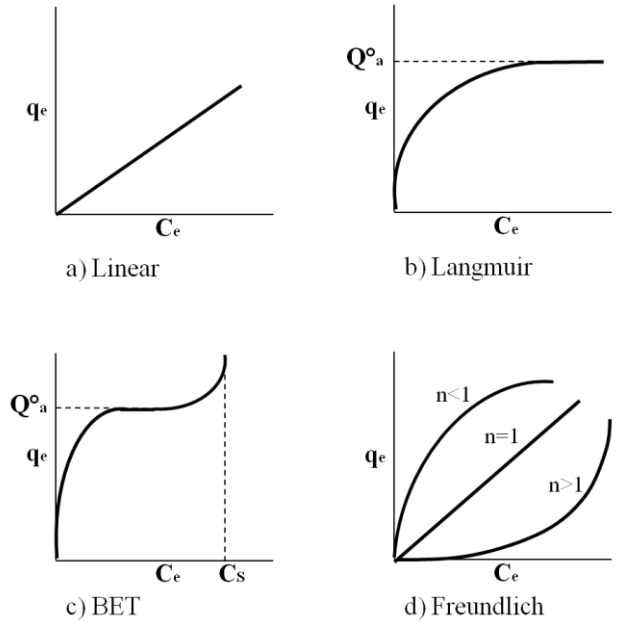

Figure 4-3: Four of the most common adsorption equilibriums: Linear (a), Langmuir (b), BET(c) and Freundlich (d).

BET isotherm

The BET isotherm is a more general multi-layer model, which assumes that a Langmuir isotherm applies to each layer and that no migration occurs between layers. This does not mean that a layer has to be completed before the next layer starts to fill up. The difference between the Langmuir model and the BET model is illustrated in figure 4-4. An assumption is also made for the different layers of the BET model, which is that there is equal energy of adsorption for all layers except for the first layer. The BET equation can be described as in equation 4.4:

$$q = \frac{q_m K_B C}{(C_s - C)\left[1 + (K_B - 1)\cdot\frac{C}{C_s}\right]} \qquad (4.4)$$

Where K_B is a constant related to the binding intensity for all layers, and C_s is the concentration of solute when all layers are saturated.

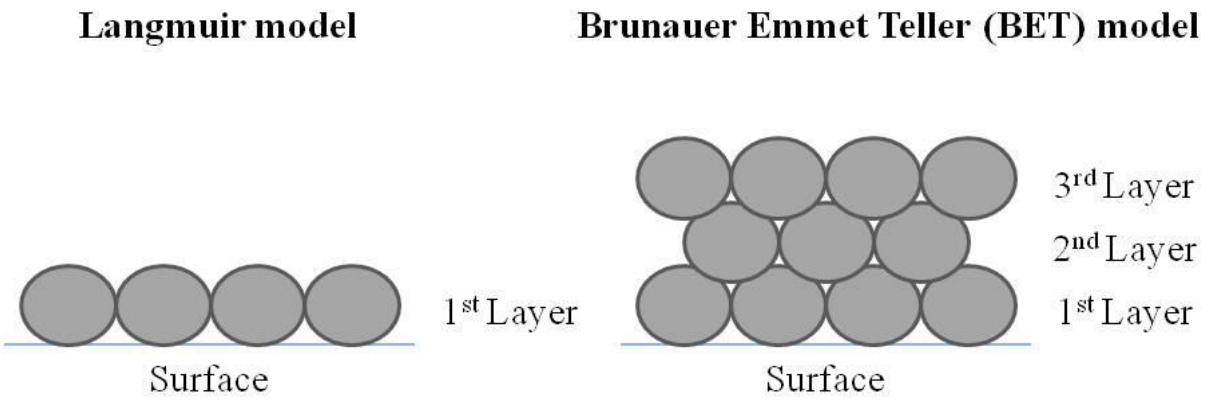

Figure 4-4: The Langmuir model assumes that the adsorbents adsorb in a monolayer. However, the BET model assumes multilayers.

Freundlich isotherm

The Freundlich isotherm is an empirical model which describes the relation between the weight of solute adsorbed per unit weight of solid (w), and the concentration of solute in the solution at equilibrium (c). The relation is described in equation 4.5:

$$w = \alpha c^n \qquad (4.5)$$

Where α and n are constants. The equation is an outcome of the consideration of heterogeneity of the surface, when applied to the adsorption of vapours on solid. The isotherm makes no assumption for the reversibility of adsorption, as opposed to the Langmuir isotherm. For the case of adsorption from solution, it is possible but not proven that the surface is heterogeneous if the adsorption data fits the equation (Adamson, 1982).

5. Materials and methods

For the experimental part, a model solution was used for the NA in crude oil. 4-heptylbenzoic acid was used as the model NA and octane was used as the model crude oil. All solutions were prepared with ultrapure Milli-Q water, and all instruments and equipment are listed in appendix 9.1.

5.1 Materials

Aqueous ammonium hydroxide, octane (98 %), ethanol (96 %), iron(II)chloride (98 %), iron(III)chloride (97 %), hydrochloric acid (37 %), tetraethyl orthosilicate (98 %), 4-heptylbenzoic acid and sodium hydroxide were all reagent grade and purchased from Sigma-Aldrich (Germany). SiO_2-MAG paramagnetic unmodified particles (5 % w/v) were purchased from microParticles Research and Development Laboratory (Germany).

5.2 Methods

5.2.1 Synthesis of Fe_3O_4 nanoparticles by co-precipitation

Fe_3O_4 nanoparticles were synthesized by co-precipitation (Zhang, et al., 2007): a mixture of $FeCl_3$ (20mL, 1M in 0,2M HCl) and $FeCl_2$ (20 mL, 0,5M in 0,2M HCl) was added dropwise to a mechanically stirred solution of sodium hydroxide (200 mL, 1,5 M) within 5 minutes under an inert nitrogen atmosphere at 80 °C. The mixture was stirred (approx. 200 rpm) for 20 minutes at 80 °C (MR 3004 Safety, Heidolph) and subsequently cooled to ambient temperature. The sediment was separated by an external magnetic field, and washed three times with deionized water. After the washing of the Fe_3O_4 MNP, the volume of water and particles was about 1 liter, and was reduced with a rotavapor (Laborota 4003, Heidolph). Then the Fe_3O_4 MNP in water were centrifuged (Centrifuge 5810, Eppendorf) at 4000 rpm in 10 minutes, but all the particles did not sediment. The chemical reaction of the co-precipitation is shown in equation 5.1:

$$Fe^{2+}(aq) + 2Fe^{3+}(aq) \rightarrow Fe_3O_4(s) + 2H^+(aq) \quad (5.1)$$

The concentration of the Fe_3O_4 MNP in water was found by measuring 2-3 g of suspension in a snap-cap vial, and heating it up to 60 °C. The exact weight of the snap-cap vial and suspension was noted before heating, and then weighed again several times as the water started to evaporate.

5.2.2 Coating of the Fe_3O_4 nanoparticles with silica

To protect the particles and to make them available to further functionalizing, a silica-coating was formed on the Fe_3O_4 MNP via a sol-gel approach. The sol–gel process has been adopted more widely for preparation of silica-coated MNP for its advantages compared with the other methods: relatively mild reaction condition, low cost and surfactant-free.

The silica coating is fabricated on the surface of the Fe_3O_4 MNP through a sol–gel approach according to Deng, et al., 2005 with some modifications. Fe_3O_4 nanoparticles (0,1 g) were dispersed in the mixture of ethanol (80 mL), deionized water (20 mL) and aqueous ammonia (1,0 mL) after being activated with 50 mL of HCl solution (0,1 M) under ultrasonication for approximately 25 minutes. Then, 0,2 mL of tetraethyl orthosilicate (TEOS) was added into the mixture, followed by stirring (450 rpm) at room temperature for 6 hours. After washing with ethanol and water several times, the obtained Fe_3O_4/SiO_2 MNP were stored in water at room temperature and then dried at 60 °C under nitrogen. The chemical reaction from TEOS to silicon dioxide is stated in equation 5.2:

$$Si(OC_2H_5)_4 + 2H_2O \rightarrow SiO_2 + 4C_2H_5OH \quad (5.2)$$

5.3 Characterization of the MNP

5.3.1 Dynamic light scattering (DLS)

SiO_2-MAG paramagnetic unmodified particles were purchased from microParticles Research and Development Laboratory (Germany), in a 5 % w/v aqueous suspension. The size needed to be determined, since the size-range of the commercial particles was too large (size 1-10 μm).

The nanosizer (Nano ZS Zetasizer Nanoseries Malvern instruments) measures particle and molecule size from below a nanometer to several microns using dynamic light scattering (DLS). The technique uses light which is scattered by the particles, and the intensity of scattered light is detected. If the particles were stationary, the light scattering would be constant. The diffusion of the diluted particles is measured as they move under Brownian motion, and this is converted to size by the usage of Stokes-Einstein relationship (Hiemenz & Rajagopalan, 1997):

$$D = \frac{k_B T}{6\,\pi\,\eta\,R_S} \tag{5.3}$$

Where ŋ is the viscosity of the fluid, k_B is the Boltzmann constant, R_S is the radius of the sphere, T is the temperature and D is the diffusion coefficient.

30 μL from the SiO_2-MAG 5 % w/v aqueous suspension was diluted by 3 mL of water. The diluted suspension was analyzed in the nanosizer (Malvern instruments) at 25 °C.

5.3.2 Digital Video Microscopy (DVM)

Another way to estimate the particle size is by microscopy. The method was used on the commercial SiO_2-MAG particles. A drop of the diluted suspension of particles was placed between two glass disks, and analyzed with a microscope (Eclipse ME600, Nikon) fitted with a camera (CoolSNAP-Pro, Media cybernetics) at a magnification of 50 times.

5.3.3 Gas adsorption

The Brunauer-Emmet-Teller (BET) method was used to determine the specific surface area of the synthesized particles. The method is based on the adsorption of gas on the surface of the particles, and measuring the amount adsorbed gas at known pressure. By analyzing a known amount of particles, the specific surface area can be found. The BET value can be defined as the surface area per mass of particles, as described in equation 5.4:

$$BET = \frac{Surface\ area\ (m^2)}{mass\ (g)} \tag{5.4}$$

The analysis was executed by weighing the BET sample tube, and then loading minimum 50 mg of sample in the tube. The exact weight was noted. The tube was sat in the cooled location of the smartprep degassing rack, and a lid was placed on the open top to achieve approximately 200 mTorr at room temperature. The sample tube was placed carefully in the heated location of the rack, at 300 °C overnight, to remove any adsorbed contaminants from the surface of the particles before analysis. The sample tube was removed from the heat, cooled down, and the lid was carefully removed. The tube was then placed in the sample port of the gas adsorption analyzer (TriStar 3000, Micromeritics Instrument Corporation), and liquid nitrogen was placed under the tube during the analysis. The measured weight of the sample was entered in the software (Version 6.04, Micrometitics Instrument Corporation), and the BET value was calculated. A scheme of the method is presented in figure 5-1.

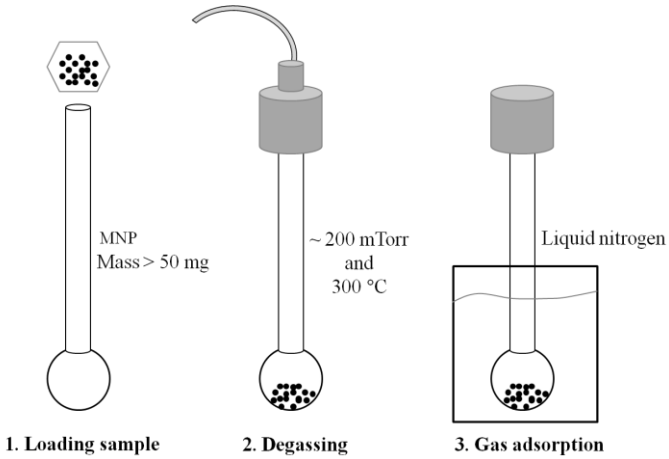

Figure 5-1: A scheme of the gas adsorption analysis, from loading the sample (1), degassing the MNP (2) to the gas adsorption analysis (3).

5.3.4 X-ray diffraction

X-ray diffraction (XRD) is used to determine the crystallinity of a compound, which is either in solid, powder or liquid form. The analysis investigates atomic arrangement, orientation, imperfections, and provides information on structures and phases. An unknown sample can be identified by comparing the XRD pattern with standard reference patterns and measurements. The advantages of XRD are the rapidity of measurement, simplicity of sample preparation, non-destructive technique and the analysis can be used for mixed phases (e.g. soil).

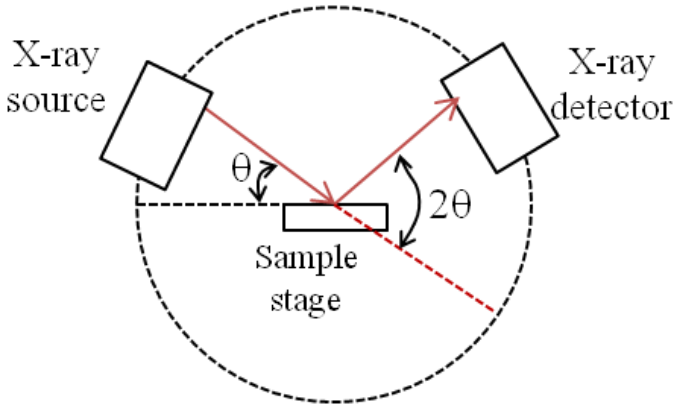

Figure 5-2: The XRD instrument consists of a X-ray source, a sample stage and a moving X-ray detector which record the directions and intensities of the outgoing diffracted waves.

An X-ray source creates an oscillating electric field of an incident x-ray, which moves the atomic electrons and their accelerations generate an outgoing wave as illustrated in figure 5-2. Figure 5-3 gives an overview of the parameters of Bragg's law (eq. 5.5), which describes the relation between the angle of incidence of the two parallel rays (Θ), the interplanar spacing (d) and the wavelength (λ) (Fultz & Howe, 2013):

$$2d\ sin\Theta = \lambda \tag{5.5}$$

Constructive wave interference occurs when the difference in path length for the top and bottom rays is equal to one wavelength (Fultz & Howe, 2013).

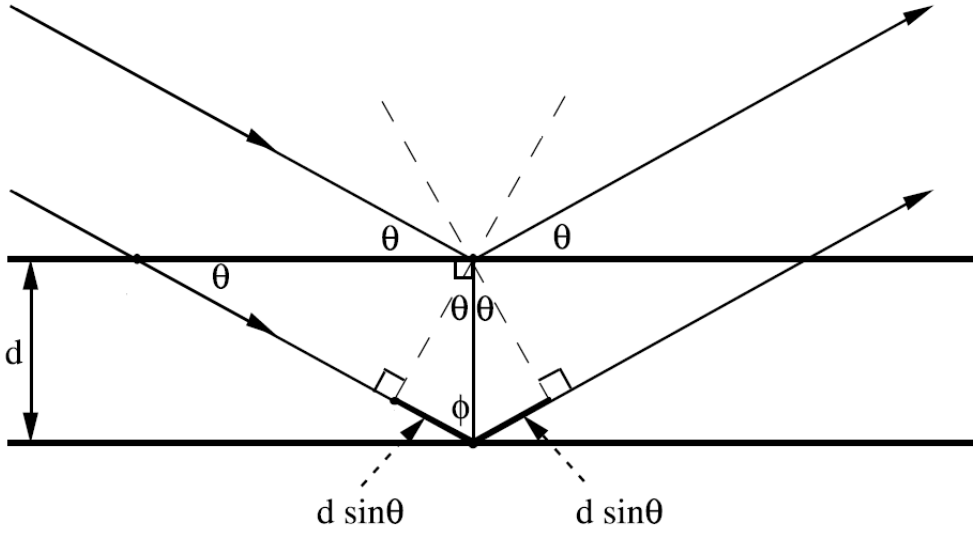

Figure 5-3: Parallel incident rays with angle, Θ, scattered from two planes, separated by a spacing (d) (Fultz & Howe, 2013).

The Scherrer equation is a relationship (eq. 5.6) between the size of nanoparticles and the broadening of a peak in a diffraction pattern, and is used to determine the size of particles of crystals in the form of powder (Langford & Wilson, 1978)

$$\tau = \frac{K\,\lambda}{\beta \cos\theta} \tag{5.6}$$

Where τ is the mean size of the ordered crystalline domains, K is a dimensionless shape factor, β is the line broadening at half the maximum intensity and Θ is the Bragg angle.

The XRD instrument was used to check if the compound in the synthesized MNP core was actually Fe_3O_4, and to estimate the size of the MNP. The samples were made into a fine grain powder with a mortar and pestle before analysis, and transferred into a sample container. The samples were analyzed with a X-ray diffractometer (D8 Advance DaVinci, Bruker) for 30 minutes with a constant slit width.

5.4 UV-vis spectroscopy

Ultraviolet-visible (UV-vis) spectroscopy was used to determine the concentration of NA in octane after adsorption with MNP. The electromagnetic spectrum is illustrated in figure 5-4, and the UV and visible region is indicated. During an analysis, the UV-vis light will pass through the sample with continuously changing wavelength. The sample absorbs the light with the wavelength which corresponds to the energy level required to excite an electron to a higher level (McMurry, 2008).

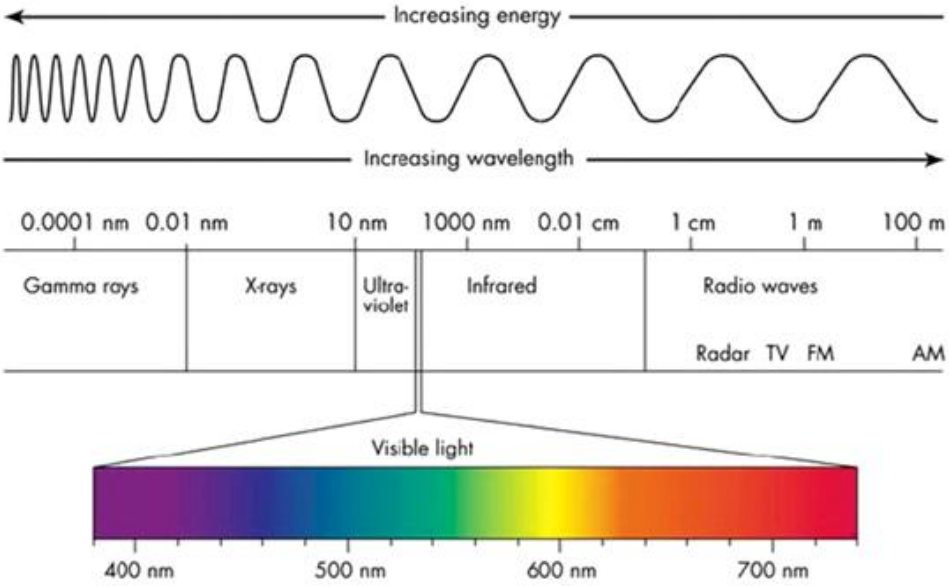

Figure 5-4: Ultraviolet (UV) light covers the range of 190 to 400 nm and visible (vis) covers the range of 400 to 800 nm wavelengths in the electromagnetic spectrum (Cole-Parmer, 2015).

The measured absorbed light can be used to find the concentration (c) of an absorbing species in solution by the usage of the Beer-Lambert-Law, as described in equation 5.7:

$$A = \log\left(\frac{I_0}{I}\right) = \varepsilon\, c\, l \qquad (5.7)$$

Where A is the absorbance, I_0 is the intensity of the incident light at a given wavelength, I is the transmitted intensity, l is the path length through the sample and ε is the molar absorptivity or also called extinction coefficient (Ingle & Crouch, 1988).

This method was utilized on the model NA, 4-heptylbenzoic acid, which is illustrated in figure 5-5 (A). The NA molecule absorbed UV-vis light, since it has a conjugated system. The solvent, octane, is also illustrated in figure 5-5 (B). Octane has no double bonds, only a straight chain of eight carbon atoms, which enables the NA to be detected. The UV-vis Recording Spectrophotometer (UV-2401PC, Shimadzu) was utilized to analyze all samples. Quartz cuvettes (Precision cells, Hellma Analytics) were chosen due to the use of organic solvent.

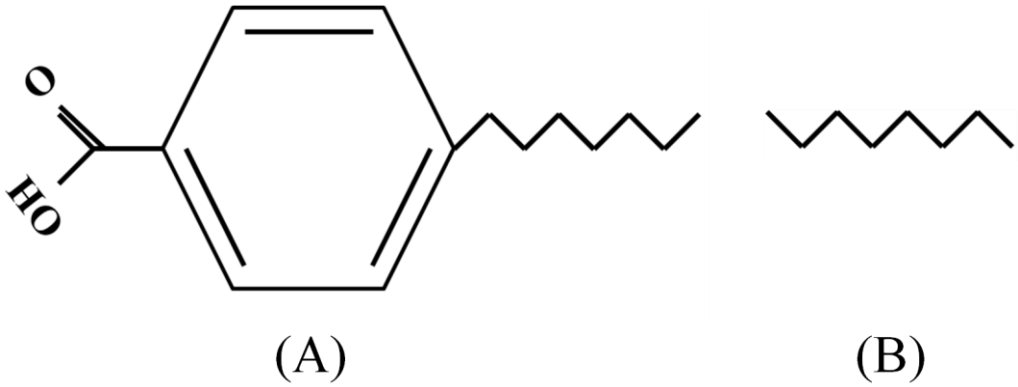

Figure 5-5: The model NA, 4-heptylbenzoic acid (A), and the model oil, octane (B).

5.4.1 Calibration curve for NA in octane

To find the exact concentration of NA in octane, a calibration curve was made by measuring UV-vis absorption at known NA concentrations.

Calibration curve 1

A stock solution was made by measuring NA and diluting with octane for a concentration of 2 g/L. Solutions were made from the stock solution with concentrations 4,0-18,0 mg/L and a blank solution was made with pure octane. The blank solution was used to calibrate the baseline. The UV absorption was measured for wavelengths 200-800 nm for the first solution, and then the remaining solutions was measured at 200-400 nm to find the maximum wavelength.

Calibration curve 2

A second calibration curve was made by measuring NA and diluting with octane to a concentration of 1 g/L. Solutions were made from the stock solution with concentrations 4,0-18,0 mg/L and a blank solution was made with pure octane. The blank solution was used to calibrate the baseline. The UV absorption was measured for wavelengths 200-400 nm.

5.4.2 Removal of NA from octane with Fe_3O_4/SiO_2 MNP

The synthesized Fe_3O_4/SiO_2 MNP were utilized to adsorb NA in octane, and the concentration difference before and after adsorption was measured by UV-vis spectroscopy.

A set of 10 samples was prepared with a constant amount of MNP and increasing concentrations of NA, to measure the adsorption. The previously measured value of BET (eq. 5.4) was used to approximate the amount of MNP to be used. The BET describes the specific surface area of the MNP per mass. The surface excess, Γ (eq. 5.8), was assumed to be 1 mg/m^2.

$$\Gamma = \frac{V(C_o - C_e)}{Surface\ area} \qquad 5.8$$

The volume was set at 10 mL per sample, and the concentration difference is assumed to be 0,5 g/L. By using equations 5.4 and 5.8, the mass of MNP was calculated to be 41 mg per sample. The initial concentration of NA, C_o, will be known, and the concentration at equilibrium, C_e, will be measured by UV-vis spectroscopy. The equilibrium concentration of the NA on the surface of the MNP adsorbent, q_e, can then be calculated with equation 4.2.

Test procedure for NA adsorption

A stock solution of NA in octane was made, with a concentration of 2 g/L. The MNP, octane and stock solution were measured as described in table 5.1, for a total volume of 10 mL in glass vials. The samples were placed on a shaker (IKA) for 24 hours at room temperature. The MNP were separated from the solution with a magnet produced by amazing magnets, USA.

The UV absorbance was measured at 243 nm, in a quartz cuvette. The samples were diluted with octane if the concentration of NA was too high.

Table 5.1: Blank sample with pure octane, reference sample with MNP and pure octane, and 10 samples with MNP, octane and NA with increasing concentration for the test procedure.

Sample ID	MNP (mg)	Octane (g)	Stock solution (g)	Concentration NA (g/L)
Blank	0	7,03	0,00	0,0
Reference	41	7,03	0,00	0,0
1	41	6,33	0,70	0,2
2	41	5,62	1,41	0,4
3	41	4,92	2,11	0,6
4	41	4,22	2,81	0,8
5	41	3,52	3,52	1,0
6	41	2,81	4,22	1,2
7	41	2,11	4,92	1,4
8	41	1,41	5,62	1,6
9	41	0,70	6,33	1,8
10	41	0,00	7,03	2,0

Procedure 1.1

The Fe_3O_4/SiO_2 MNP were dispersed in octane and shaken for 24 hours, to rinse the particles and thus assure that the MNP do not contaminate the samples during adsorption. Then the particles were separated from the octane and dried under nitrogen at 60 °C until constant mass. For the NA adsorption, 80 mg of MNP were utilized.

A stock solution of NA in octane was made, with a concentration of 2 g/L. The MNP, octane and stock solution were measured as described in table 5.2, for a total volume of 5 mL in glass vials. The samples were placed on a shaker (IKA) for 24 hours at room temperature. The MNP were separated from the solution with a magnet produced by amazing magnets, USA. The UV absorbance was measured at 243 nm, in a quartz cuvette. The samples were diluted with octane if the concentration of NA was too high.

Table 5.2: Blank sample with pure octane, reference sample with MNP and pure octane, and 5 samples with MNP, octane and NA with increasing concentration for procedure 1.1.

Sample ID	MNP (mg)	Octane (g)	Stock solution (g)	Concentration NA (g/L)
Blank	0	3,52	0,00	0,0
Reference	80	3,52	0,00	0,0
1	80	3,16	0,35	0,2
2	80	2,11	1,41	0,8
3	80	1,41	2,11	1,2
4	80	0,70	2,81	1,6
5	80	0,00	3,52	2,0

Procedure 1.2

Procedure 1.1 for adsorption with Fe_3O_4/SiO_2 MNP was repeated, but the number of samples was increased from 5 to 7. The MNP, octane and stock solution were measured as described in table 5.3

Table 5.3: Blank sample with pure octane, reference sample with MNP and pure octane, and 7 samples with MNP, octane and NA with increasing concentration for procedure 1.2.

Sample ID	MNP (mg)	Octane (g)	Stock solution (g)	Concentration NA (g/L)
Blank	0	3,52	0,00	0,0
Reference	80	3,52	0,00	0,0
1	80	3,16	0,35	0,2
2	80	2,81	0,70	0,4
3	80	2,11	1,41	0,8
4	80	1,41	2,11	1,2
5	80	1,05	2,46	1,4
6	80	0,70	2,81	1,6
7	80	0,00	3,52	2,0

6. Results and discussion

Commercial MNP were purchased to examine the possibility of their application for further functionalization, and are therefore a natural starting point of the results. Thereafter, results from the synthesized MNP are presented.

6.1 Characterization of the commercial silica-covered MNP

The SiO_2-MAG paramagnetic particles were originally in aqueous solution, and had a concentration of 5 %. The particles sedimented in the bottle, as shown in figure 6-1 (A), and left a clear water phase on top. When carefully applying a magnet to the side of the bottle with particles, the sedimented layer on the bottom was attracted to the magnet, as shown in in figure 6-1 (B and C). The size of the particles was planned to be estimated by nanosizer, but was replaced by microscopy.

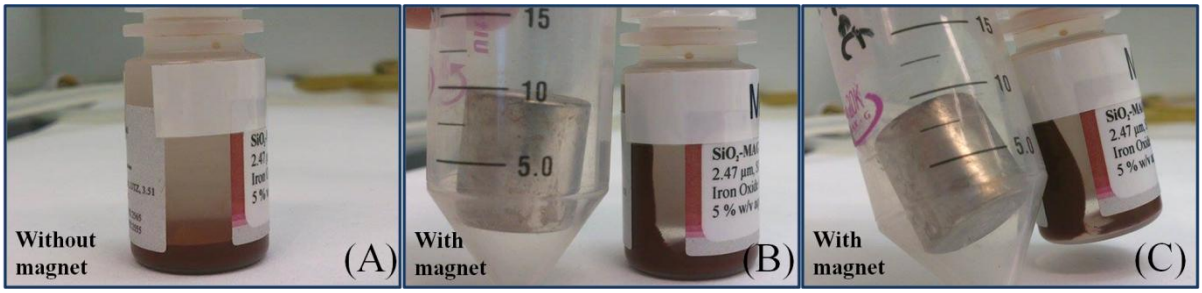

Figure 6-1: Sedimented magnetic nanoparticles (A), and particles moving in the bottle after placing the magnet closer (B and C).

6.1.1 Dynamic light scattering

The SiO_2- MAG particles were diluted to 0,05 % concentration with MilliQ water, and analyzed in the nanosizer. The measurement took several minutes, as indicated in table 6.1. Also, the instrument used additional time to prepare after the cuvette was inserted. When the cuvettes were taken out from the instrument, the particles had sedimented. The sedimentation was indicated by a clear layer with pure water at the top, and a vague colouring of red in the bottom of the cuvette. The results were not satisfying, and a new method was considered.

Table 6.1: The commercial silica covered MNP were analyzed in the nanosizer to determine the size of the particles. 3 parallels (1.1-3, 2.1-3 and 3.1-5).

Record	Time of measurement	Z-Ave (d.nm)	Pk 1 Mean Int (d.nm)
1.1	13:28	1648	1005
1.2	13:31	2124	2406
1.3	13:34	3176	3060
2.1	13:47	1384	639,9
2.2	13:50	1655	1286
2.3	13:53	2114	2420
3.1	13:58	3649	2879
3.2	14:00	3567	2602
3.3	14:02	3601	2194
3.4	14:04	4325	1636
3.5	14:06	4228	1545

6.1.2 Digital video microscopy (DVM)

A drop of the diluted particles in 0,05 % solution was placed between two glass disks, and analyzed in a the DVM. A magnification of 50 times made it possible to look at the individual particles, and pictures were taken as shown in figure 6-2 (A-C).

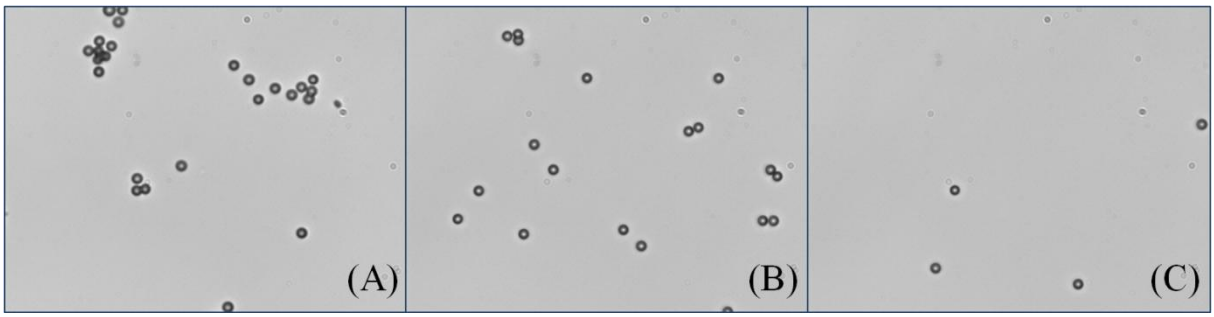

Figure 6-2: Samples of the 0,05 % MNP in aqueous solution were analyzed in a microscope. Pictures (A-C) were taken of the MNP in 50 times magnification.

A total of six pictures were used to estimate the average diameter of the commercial SiO_2-MAG particles, which combined made up a count of 116 particles. The software Image proplus 5.0 was used to calculate the diameter, taking into account the magnification of the microscope (table 6.2).

Table 6.2: The commercial MNP analyzed with a DVM and average particle sizes.

Parameter	Value
Number of pictures	6
Total number of MNP counted	116
Magnification	50
Average radius ratio	1,1
Average diameter (µm)	3,3
Surface area (μm^2)	20,6

The approximate value for the MNP mass needed to achieve a surface excess of $1 mg/m^2$ and a change in NA concentration of 0,5 g/L after adsorption, was calculated to be 11,7 g for each sample with a volume of 5 mL. Because the concentration of the MNP dispersion is 5 w/w %, the amount needed for adsorption is equal to 234 g of dispersion. This amount of particles in each sample is too high, which means that the particles are too big. The density of the Fe_3O_4 MNP was assumed to be equal to the theoretical value of Fe_3O_4 (5,1 g/cm^3) at 25 °C, so the specific surface area was calculated to be 1,4 m^2/g. To increase the surface area for adsorption, and therefore decreasing the amount of needed MNP, it was decided to synthesize Fe_3O_4 MNP in the laboratory by the method of co-precipitation.

6.2 Synthesis of MNP

The MNP were synthesized and coated with a layer of silica in more than one batch, and the identification of the various MNP is listed below in table 6.3.

Table 6.3: The several batches of Fe_3O_4 MNP with and without silica coating with identification names.

Synthesis	First Fe_3O_4	Second Fe_3O_4
No SiO_2	MAG1	MAG2
SiO_2 Test	SiO_2MAG1.1	-
SiO_2 upscale	SiO_2MAG1.2	SiO_2MAG2.1

6.2.1 Synthesis of Fe_3O_4 magnetic core

The magnetic core of the MNP was successfully synthesized by co-precipitation, and showed signs of magnetic properties when a magnet was held against the tube wall, as illustrated in figure 6-3. The volume of the MAG1 suspension was increased to approximately 1 L because of the washing, and needed to be reduced. It was first centrifuged, which was not successful. The suspension was still completely black, and there was no grading of transparency. Instead, the suspension volume was decreased by evaporating the water with a rotavapor.

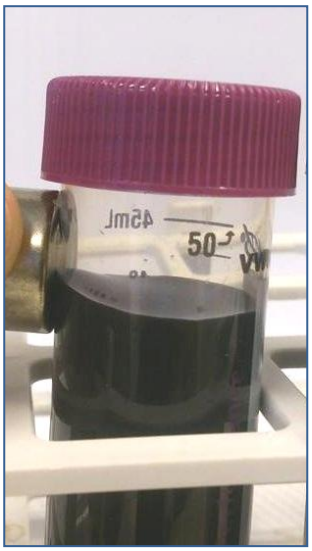

Figure 6-3: The synthesized Fe_3O_4 MNP in deionized water (MAG1).

The concentration of Fe_3O_4 MNP was found by measuring 2,6180 g of suspension, and placing it in a heating block at 60 °C to evaporate water. The weight of the suspension was regularly measured until it was constant. This is illustrated in figure 6-4. Only the weight of the Fe_3O_4 MNP was left when the suspension weight was constant and the water had evaporated.

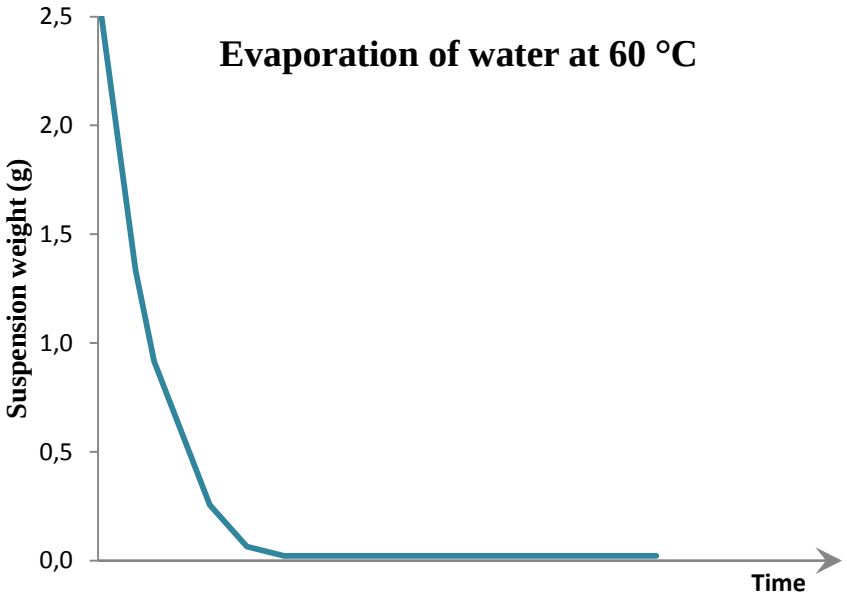

Figure 6-4: The suspension weight decreased until it was stable, when water was evaporated at 60 °C.

The Fe_3O_4 MNP left in the snap-cap vial were weighed to be 0,022 g (figure 6-5), and the concentration of the suspension was then calculated to be 0,84 % w/w (table 6.4).

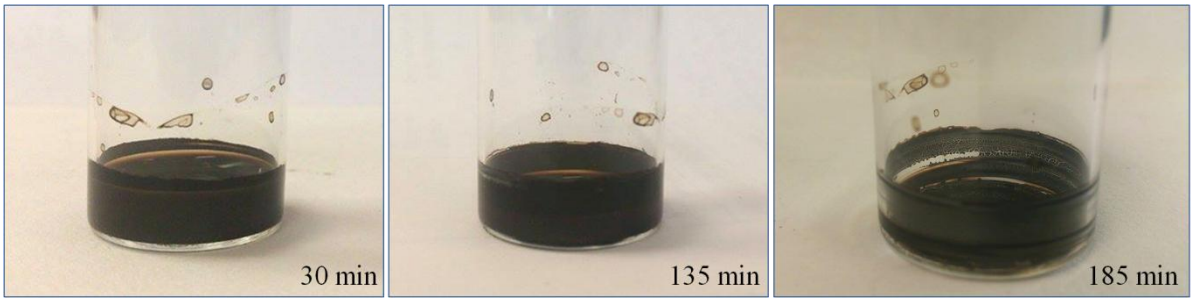

Figure 6-5: Suspension of Fe_3O_4 MNP in snap-cap vial at 60 °C, while water evaporated to determine the concentration of MNP. 30 minutes, 135 minutes and 185 minutes after start.

The synthesis of Fe_3O_4 MNP was repeated to produce more MNP for the experiments. The synthesized MAG2 were significantly easier to separate with magnet this time, and an increase in concentration with a rotavapor was not needed. The Fe_3O_4 MNP suspension before and after separation with magnet are illustrated in figure 6-6.

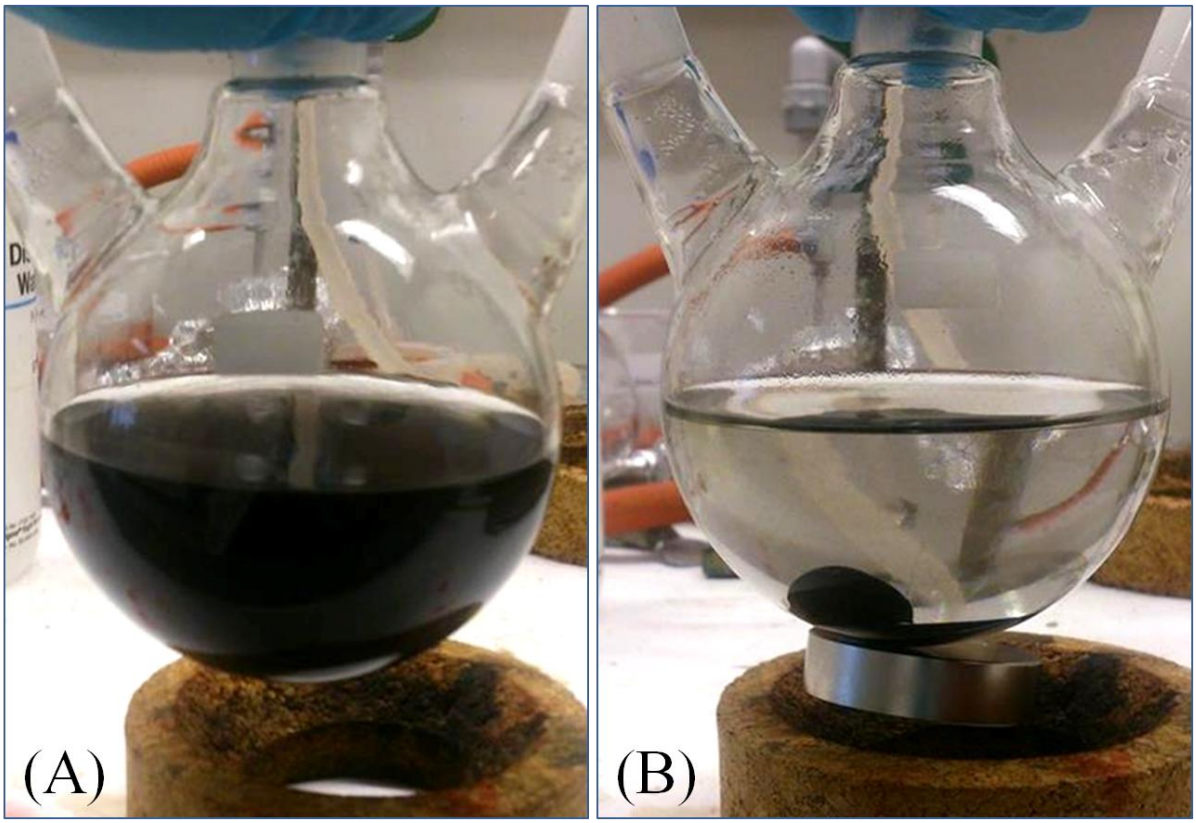

Figure 6-6: The synthesized Fe_3O_4 MNP (MAG2) before (A) and after applying a magnet beneath the flask (B).

The theoretical mass of the synthesized Fe_3O_4 MNP was calculated, and compared with the real mass as listed in table 6.4. The calculated yield was 72 % for the MAG1, which can be explained by the loss of particles during washing with water after synthesis. The MNP were difficult to remove from the water, and the wastewater was still brown when discarded. After the second synthesis, the MAG2 were much easier to separate, and the yield was calculated to be 109 %. The MNP concentration for MAG2 was found by the same method as described for the MAG1 synthesis, and the collected results are given in table 6.4.

Table 6.4: The calculated theoretical mass of the synthesized MNP, measured concentration and calculated yield.

Synthesis of Fe_3O_4	**MAG1**	**MAG2**
Theoretical mass (g)	2,323	2,312
Concentration (w/w %)	0,84	2,79
Yield (%)	**72**	**109**

6.2.2 Formation of silica-coating on the Fe_3O_4 MNP

Since the Fe_3O_4 MNP were dispersed in water, and not dried as requested from the method, the amount of suspension needed to achieve 0,1 g of MNP was calculated from the concentration in table 6.4. The correct amount of MNP suspension was measured and mixed with 50 mL HCl (0,1 M). The amount of water added was corrected regarding to the amount of water already present in the MNP suspension.

The MAG1 were very difficult to separate from the liquid media before coating with silica, and they did not separate when placing a magnet on the side of the bottles. After the silica-coating (SiO_2MAG1.1), the MNP were separated by placing a magnet beneath the flask, and pouring out the liquid when washing with water and ethanol (figure 6-7).

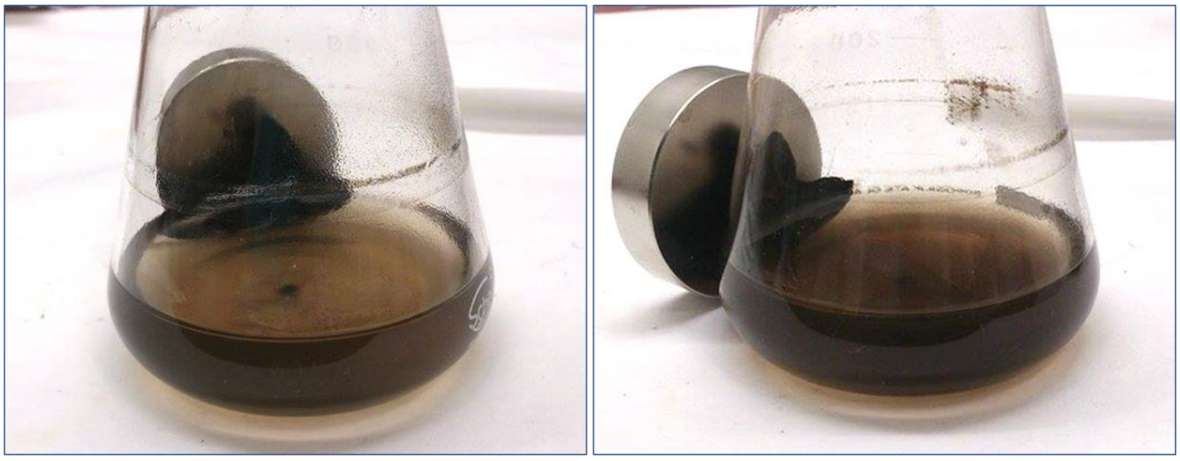

Figure 6-7: The separation of Fe_3O_4/SiO2 MNP and liquid was done by placing a magnet outside of the flask after the silica-coating (SiO_2MAG1.1).

The SiO_2MAG1.1 particles were dried at 60 °C, until the mass was constant as described in section 6.3.1. These MNP were used for characterization, so the covering of MNP with silica was scaled up (SiO_2MAG1.2). All chemicals were tripled, except the water which was reduced regarding the water content in the MNP suspension, and the executed in 4 batches. The upscale silica covering was also executed for the MAG2 particles (SiO_2MAG2.1). The original Fe_3O_4 MNP weight before silica synthesizing, the theoretical Fe_3O_4/SiO_2 MNP weight and the measured weight of the synthesized Fe_3O_4/SiO_2 are listed in table 6.5.

Table 6.5: The original Fe_3O_4 MNP weight before silica synthesizing, the theoretical Fe_3O_4/SiO_2 MNP weight and the measured weight of the synthesized Fe_3O_4/SiO_2.

	SiO_2MAG1.1	SiO_2MAG1.2	SiO_2MAG2.1
Dry Fe_3O_4 MNP (g)	0,100	1,203	1,198
Theoretical Fe_3O_4/SiO_2 mass (g)	0,1539	1,8483	1,8433
Measured Fe_3O_4/SiO_2 mass (g)	0,1426	1,8905	1,6618
Yield (%)	**93**	**102**	**90**

6.3 Characterization of synthesized MNP

6.3.1 Gas adsorption analysis

The Brunauer-Emmet-Teller (BET) method was used to determine the specific surface area of the particles. The MNP were measured in two parallels, and the BET value was calculated from the computer software. The results are summarized in table 6.6. The BET value for the second SiO_2MAG1.1 sample may be of somewhat lower confidence than the other samples, because the sample should be at least over 50 mg.

Table 6.6: The measured mass of the MNP samples, calculated BET and R^2 values from the BET analysis.

Sample	Mass (mg)	BET value (m^2/g)	R^2
MAG1	58,6	98,4939 ± 0,1758	0,9999
MAG1	58,2	103,8450 ± 0,1985	0,9999
SiO_2MAG1.1	55,9	121,1666 ± 0,8588	0,9991
SiO_2MAG1.1	23,5	97,0545 ± 0,5947	0,9993
SiO_2MAG1.2	58,0	127,4762 ± 0,6142	0,9996
SiO_2MAG1.2	61,5	115,5579 ± 0,5542	0,9996
MAG2	68,5	100,6635 ± 0,2531	0,9999
MAG2	70,8	102,9606 ± 0,2503	0,9999
SiO_2MAG2.1	55,8	105,4292 ± 0,6441	0,9994
SiO_2MAG2.1	54,4	104,1718 ± 0,5595	0,9995
SiO_2MAG2.1 nr.3	65,0	103,5920 ± 0,5411	0,9996
SiO_2MAG2.1 nr.3	57,4	103,3414 ± 0,5192	0,9996

Also, the SiO2MAG2.1 batch nr. 3 was measured alone, because of poor magnetic properties after the silica coating. All the MNP had a high BET value, especially compared to the low specific surface area of the commercial MNP which was 1,4 m^2/g. From that it could be concluded that the synthesized MNP were possible to test for adsorption of the model NA. The average BET value for MAG1 was calculated to be 101 m^2/g. and 121 m^2/g for the first silica cover: SiO_2MAG1.1. After the second cover, SiO_2MAG1.2, the average BET value was calculated to be 122 m^2/g. For both synthesis of silica on the MAG1, the BET value increased with approximately 20 m^2/g. The new MAG2 had an average BET value of 102 m^2/g, which is similar to the MAG1. After silica cover, SiO_2MAG2.1, the BET was 105 m^2/g and 103 m^2/g for batch nr 3. The silica synthesis seems not to have a significant change on the BET value, compared to the silica synthesis on MAG1. The BET value was further used to estimate the amount of MNP needed for the removal of NA in octane, and to calculate the surface excess after NA removal. All samples were heated up to 300 °C under vacuum over

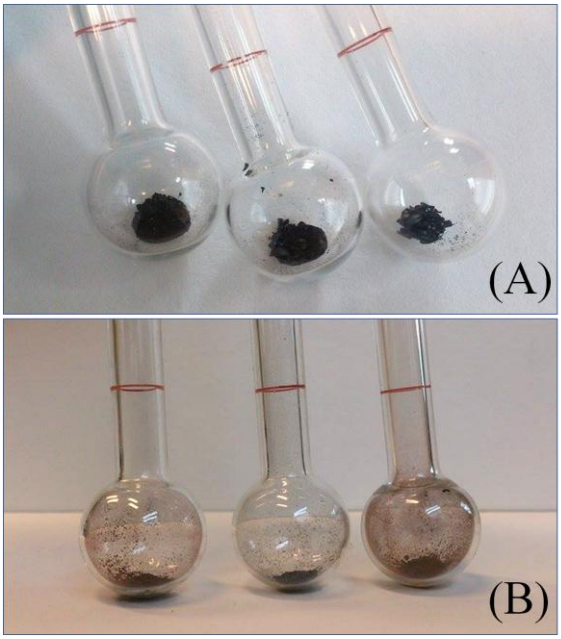

Figure 6-8: The samples (A) are exposed to 300 °C (B) before BET analysis. Samples are arranged accordingly: MAG1, MAG2 and MAG1.

night before gas adsorption analysis, and several of them changed colour during heating. All samples started out black, but after heating, the colour changed to red-brown for all samples except the MAG2 parallels. Figure 6-8 illustrates the MAG1, MAG 2 and MAG1 samples respectively, before heating (A). The MNP powders looked identical for the eye. After heating, the samples are aligned in the same order, and the colour had changed to red-brown for the MAG1 samples (B).

6.3.2 X-ray diffraction analysis

The MAG1 particles were analyzed in a XRD instrument, to make sure that the core was synthesized as Fe_3O_4 and to find an estimate of the particle size. The diffractogram in figure 6-9 is the XRD result from MAG1, and had a good comparison with standard Fe_3O_4 values (blue) when analyzed in the software (DIFFRAC.EVA). However, there was a slight shift to the left for each peak. The standard value for Fe_2O_3 (purple) did also match the MAG1 diffractogram well, and did not have a shift in the peaks.

The size of the MAG1 was estimated by using the DIFFRAC.EVA software on the peaks in the diffractogram, and using *create area* under *tools*. The start of the peak (left angle) and end of the peak (right angle) are indicated in table 6.7 with the calculated particle size for MAG1. The small peak from approximately 52 (left angle) to 55 (right angle) was not included in the calculation, because it was difficult to separate from the baseline.

Table 6.7: The left and right angle stated for each peak in the XRD diagram from MAG1 analysis, and calculated size from the area beneath the peaks from the Scherrer equation.

Peak	Left angle	Right angle	Size (Å)
1	28,995	31,999	97,7
2	32,996	37,994	114,1
3	42,301	44,202	146,1
4	56,006	58,598	112,3
5	61,602	64,194	128,3
Average			**119,7**

The estimation of particle size with a XRD diffractogram is not an exact method, but is an indicator for the size of the MNP. The average particle size of MAG1 was calculated to be 119,7 Å, approximately 12 nm.

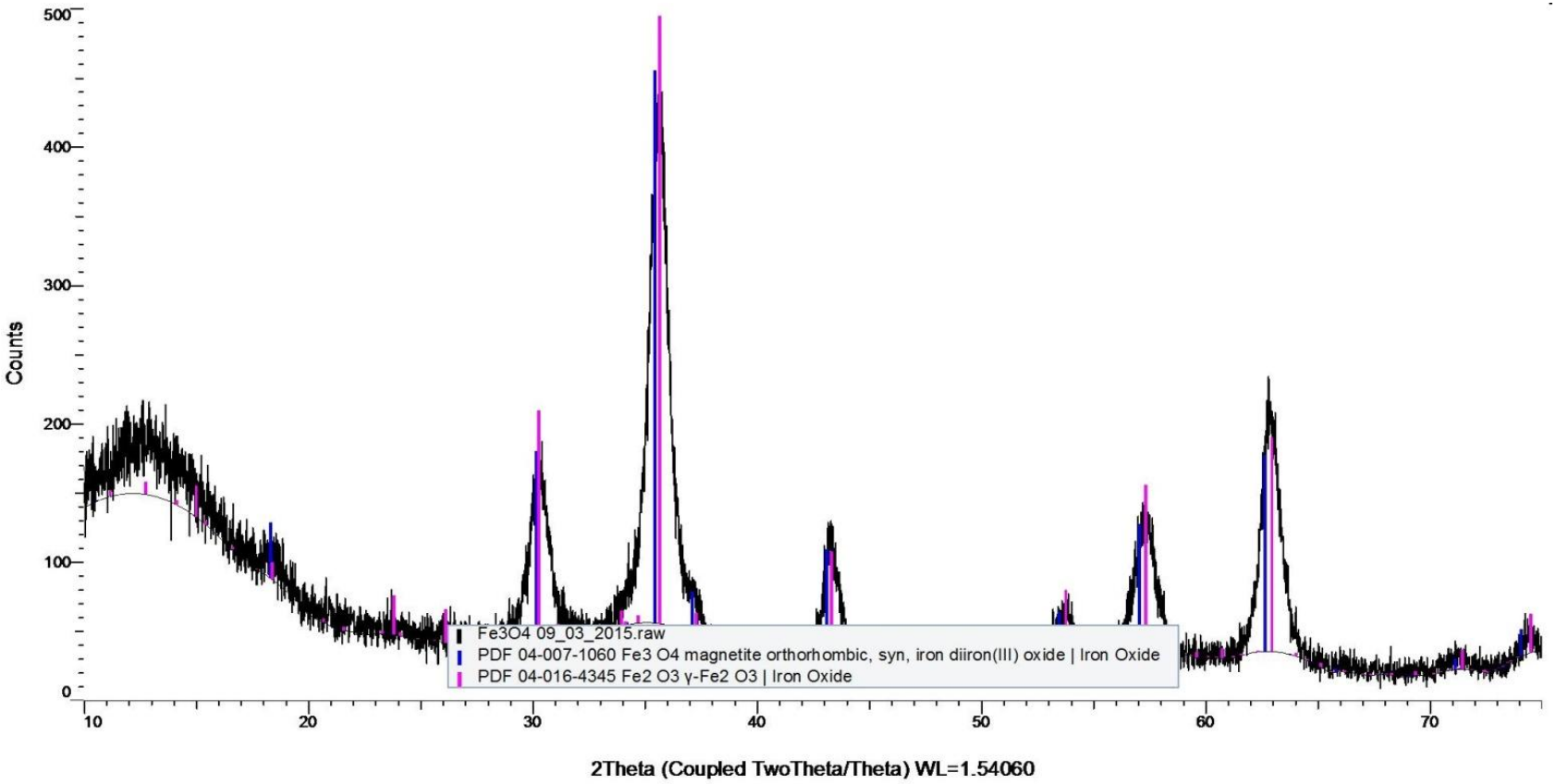

Figure 6-9: The diffractogram of the MAG1 sample (black graph). Peaks from standard diffractograms compared with the MAG1 XRD data, and the standards compatible with the MAG1 diffractogram above. The blue peaks for Fe_3O_4 (magnetite), and the purple peaks for Fe_2O_3.

The SiO_2 layer around the Fe_3O_4 core is amorphous, hence the XRD analysis of SiO_2MAG1.2 particles measures the size of the crystalline Fe_3O_4 core (figure 6-10). The size calculations were executed for these MNP as well, to compare with the MAG1 results. The start of the peak (left angle) and end of the peak (right angle) are given in table 6.8 with the calculated particle size for MAG1.

Table 6.8: The left and right angle stated for each peak in the XRD diagram from SiO_2MAG1.2 analysis, and size calculated from the area beneath the peaks from the Scherrer equation.

Peak	Left angle	Right angle	Size (Å)
1	28,995	31,507	101,0
2	33,501	37,994	98,90
3	41,995	44,494	142,6
4	56,006	58,996	123,0
5	61,004	64,500	128,9
Average			**118,9**

The average particle size from the SiO_2MAG1.2 diffractogram was calculated to be 118,9 Å, which is approximately 12 nm, and is the same value as calculated from the MAG1 diffractogram. This estimated size of the MNP was used to calculate the specific surface area, or a BET value, to compare with the BET measurements. The calculated diameter of the MAG1 from the Scherrer equation of 12 nm, results in a specific surface area of 98 m^2/g, which is close to the measured value of the gas adsorption analysis. The calculations were made with the same assumptions as for the commercial particles in section 6.1.2. The average BET value of the MAG1 was previously measured to be 101 m^2/g in section 6.3.1.

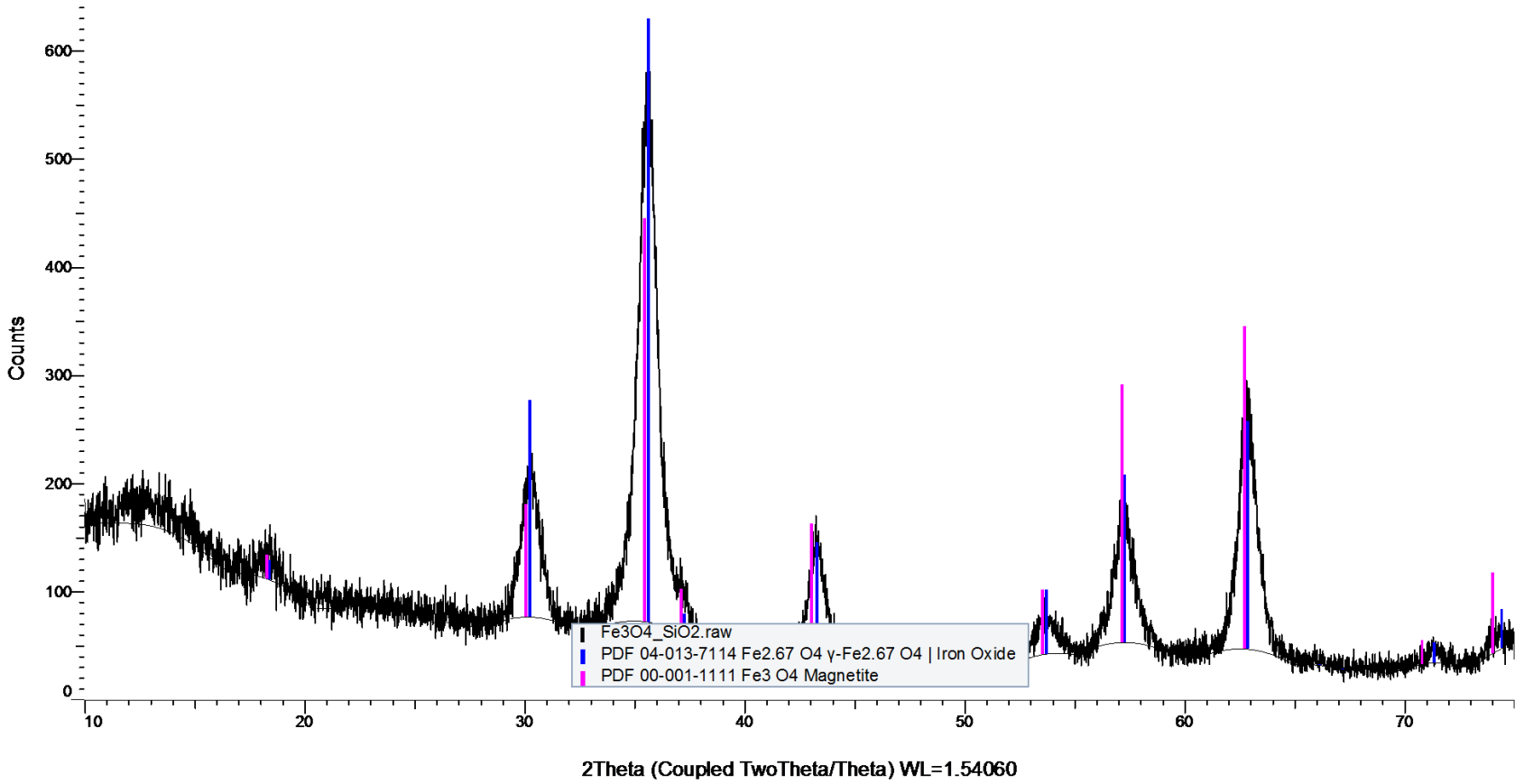

Figure 6-10: The diffractogram of the SiO_2MAG1.2 sample (black graph). Peaks from standard diffractograms compared with the SiO_2MAG1.2 XRD data, and the standards compatible with the SiO_2MAG1.2 diffractogram above. The blue peaks are for Fe_2O_4, and the purple peaks for Fe_3O_4 (magnetite).

6.4 UV-vis spectroscopy

UV-vis spectroscopy was used as the method to find the concentration of the model NA in octane. First, the solubility of NA in octane was tested: the solid, white 4-heptylbenzoic acid was shaken in a glass vial with octane for a concentration of 2 g/L. The solid was completely dissolved, as illustrated in figure 6-11.

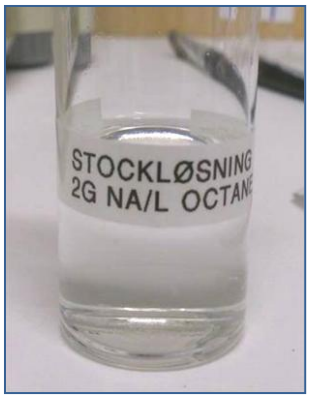

Figure 6-11: The solubility of NA in octane.

6.4.1 Calibration curve for NA in octane

Solutions with known concentrations were prepared from the stock solution, and the exact concentrations with measured absorbance are given in table 9.1 (appendix 9.2). The absorption of light with wavelength from 200 to 400 nm was measured of NA in octane at all concentrations, as shown in figure 6-12. The NA in octane were found to have a maximum absorption at a wavelength of 243 nm.

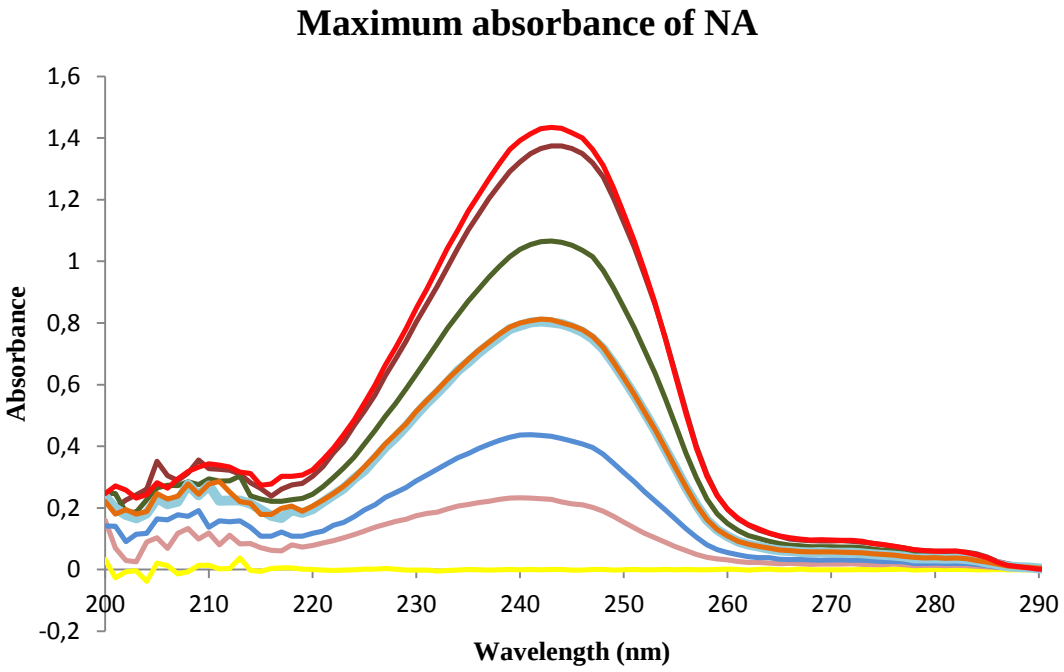

Figure 6-12: Measured absorbance plotted against wavelength for concentrations as indicated in the diagram: 0,004-0,0177 g/L (purple to red line).

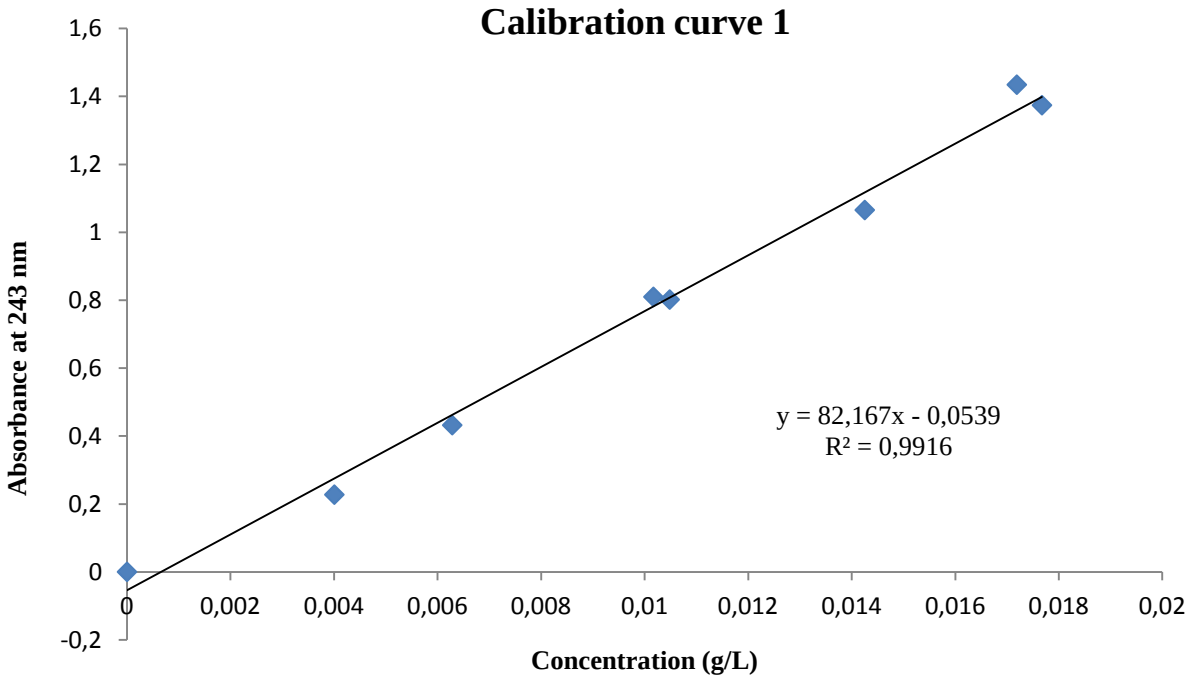

Figure 6-13: Calibration curve for the known NA concentration plotted against the measured absorbance at 243 nm.

Then the known NA concentrations were plotted against the measured absorbance at 243 nm, as illustrated in figure 6-13. The linear regression for the calibration curve did not correlate well with the data points, and was not viewed as a good calibration curve. The linear regression gave a linear function, as shown in equation 6.1:

$$A = 82{,}167C - 0{,}0539 \quad (6.1)$$

A new calibration curve was made, and the exact concentrations with measured absorbance at 243 nm are given in table 9.2 (appendix 9.2). The second calibration curve was repeated in the same linear concentration range as the first, and the accuracy was good as illustrated in figure 6-14. The linear function from calibration curve 2, equation 6.2, was used for all further UV calculations.The linear regression goes straight through all the data points.

$$A = 78{,}824C - 0{,}0085 \quad (6.2)$$

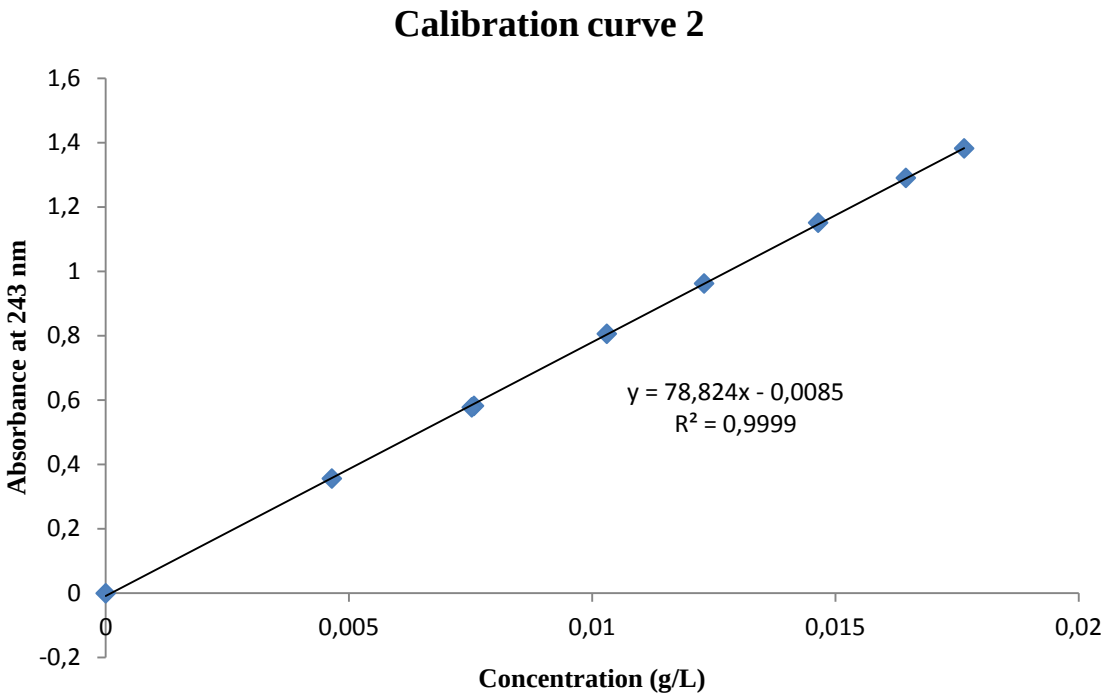

Figure 6-14: A new calibration curve made by plotting the known NA concentrations with the measured absorbance at 243 nm.

6.4.2 Removal of NA from octane

The ability to separate the Fe_3O_4/SiO_2 MNP from pure octane was tested before adding the model NA. A bottle with 7,0416 g octane and 0,0420 g MNP was shaken for 30 seconds, and then placed on a levelled surface. Some of the particles sedimented in a few seconds, but a significant amount were left in the octane and on the glass walls. When a magnet was placed outside the bottle, all the Fe_3O_4/SiO_2 MNP were immediately attracted to the magnet, as illustrated in figure 6-15.

The ability to separate Fe_3O_4/SiO_2 MNP from a solution of NA in octane was also conducted. The separation was similar to the separation of Fe_3O_4/SiO_2 MNP from pure octane, and separated completely.

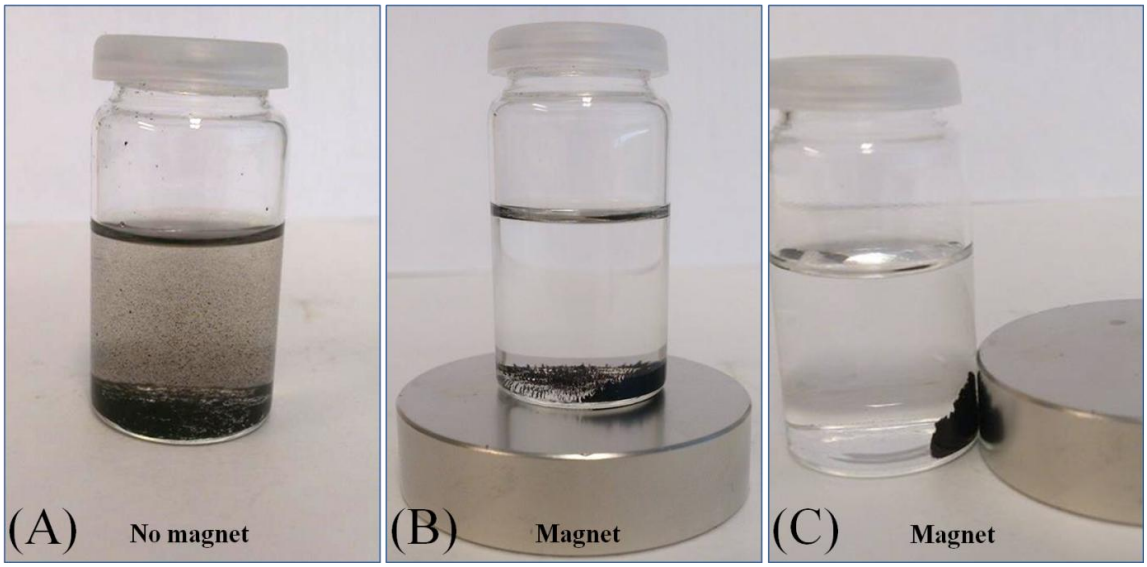

Figure 6-15: The SiO_2MAG1.2 started to sediment slightly after shaking (A), but the MNP had an immediate reaction when placed near a magnet (B and C)

Test procedure for the adsorption of NA

A test adsorption of NA from octane was executed with 41 mg MNP and a total volume of 10 mL in each of the 10 sample tubes, exact parameters are given in table 9.3 (appendix 9.2). The plotted graph of equilibrium concentration and surface excess was irregular, but had tendencies of an adsorption curve as shown in figure 9.1 (appendix 9.3). Calculated equilibrium concentration, concentration change and surface excess are given in table 6.9.

Table 6.9: The equilibrium concentration, concentration change and calculated surface excess after test adsorption with SiO_2MAG1.2.

Sample	C_e (g_{NA}/L)	ΔC (g_{NA}/L)	Surface excess (mg/m^2)
1	0,051	0,083	0,17
2	0,098	0,111	0,20
3	0,285	0,146	0,29
4	0,468	0,156	0,31
5	0,650	0,188	0,38
6	0,753	0,284	0,60
7	0,979	0,271	0,54
8	1,198	0,275	0,53
9	1,370	0,292	0,58
10	1,702	0,171	0,34

The concentration change was only from 0,083 g/L to 0,292 g/L, while it was expected to be approximately 0,5 g/L. A new procedure was made to increase concentration change and to avoid contaminations.

Procedure 1.1

The Fe_3O_4/SiO_2 MNP were dispersed in octane and shaken for 24 hours, to rinse the particles and thus assure that the MNP did not contaminate the samples during adsorption. Then the particles were separated from the octane and dried under nitrogen at 60 °C until constant mass. For the NA adsorption, 80 mg of MNP were utilized for high adsorption and thus high change in NA concentration. The total volume in the glass vials was 5 mL, also contributing to a large concentration change.

The adsorption of NA in octane with SiO_2MAG1.2 was executed for 5 samples and one reference sample without NA, and exact parameters are given in table 9.4 (appendix 9.2). UV-vis spectroscopy was used to measure the UV absorbance in the octane after NA adsorption with MNP as shown in figure 9.2 (appendix 9.3), and equation 6.2 was used to convert the measured absorbance to concentration. Equilibrium concentration, change in concentration and calculated surface excess are given in table 6.10. The equilibrium concentration was plotted against the calculated surface excess, and is shown in figure 6-16.

Table 6.10: The equilibrium concentration, concentration change and calculated surface excess after adsorption 1.1 with SiO_2MAG1.2.

Sample	C_e (g_{NA}/L)	ΔC (g_{NA}/L)	Surface excess (mg/m^2)
1	0,005	0,199	0,10
2	0,288	0,503	0,27
3	0,617	0,572	0,30
4	0,938	0,646	0,33
5	1,486	0,500	0,26

The adsorption curve shows a steady increase until approximately 0,90 g/L, where it starts to descend.

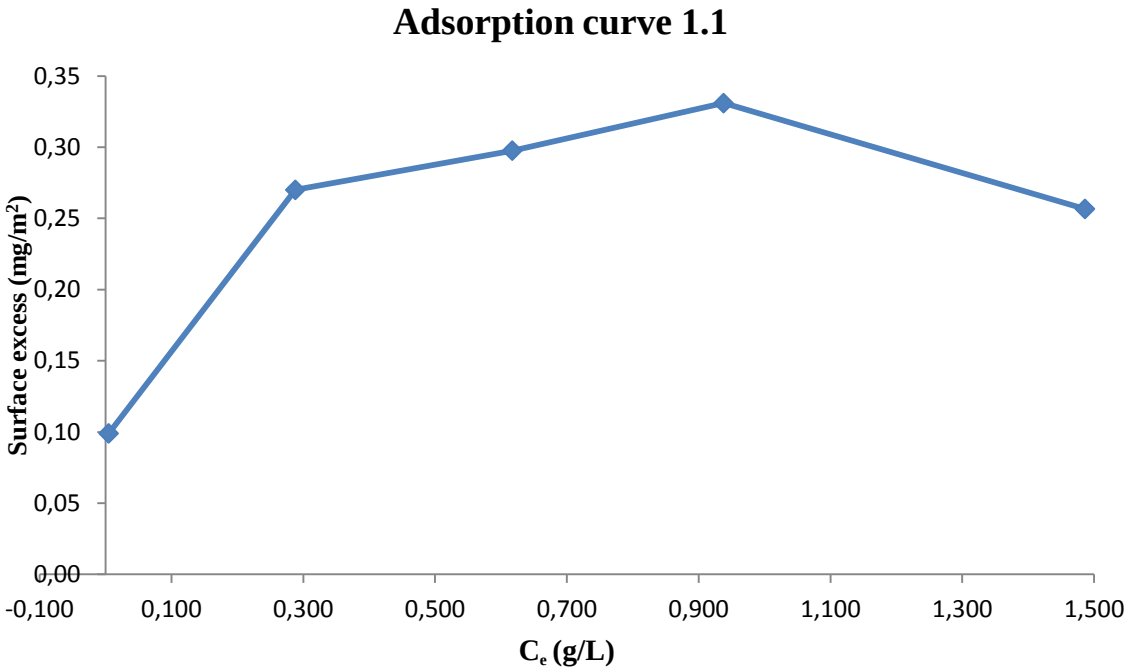

Figure 6-16: Surface excess plotted against equilibrium concentration to achieve an adsorption curve for procedure 1.1.

Procedure 1.2

Procedure 1.1 was retried with the SiO_2MAG2.1 particles. The adsorption of NA in octane with SiO_2MAG2.1 was executed for 7 samples and one reference sample without NA, and exact parameters with measured absorbance at 243 nm are given in table 9.5 (appendix 9.2).The measurements from UV-vis spectroscopy are illustrated in figure 9.3 (appendix 9.3). Equilibrium concentration, change in concentration and calculated surface excess are given in table 6.11.

The equilibrium concentration was plotted against the calculated surface excess, and is shown in figure 6-17. Results from sample 1 (first data point) may be of somewhat lower confidence, but are consistent with the data obtained from the other samples. The adsorption curve has the same steady increase at the start like procedure 1.1, but instead of declining, the graph levels and then increases again at approximately 0,90 g/L.

Table 6.11: The equilibrium concentration, concentration change and calculated surface excess after adsorption 1.2 with SiO_2MAG2.1.

Sample	C_e (g_{NA}/L)	ΔC (g_{NA}/L)	Surface excess (mg/m^2)
1	0,016	0,177	0,10
2	0,090	0,306	0,19
3	0,340	0,439	0,26
4	0,688	0,477	0,29
5	0,861	0,499	0,30
6	1,049	0,507	0,31
7	1,227	0,503	0,35

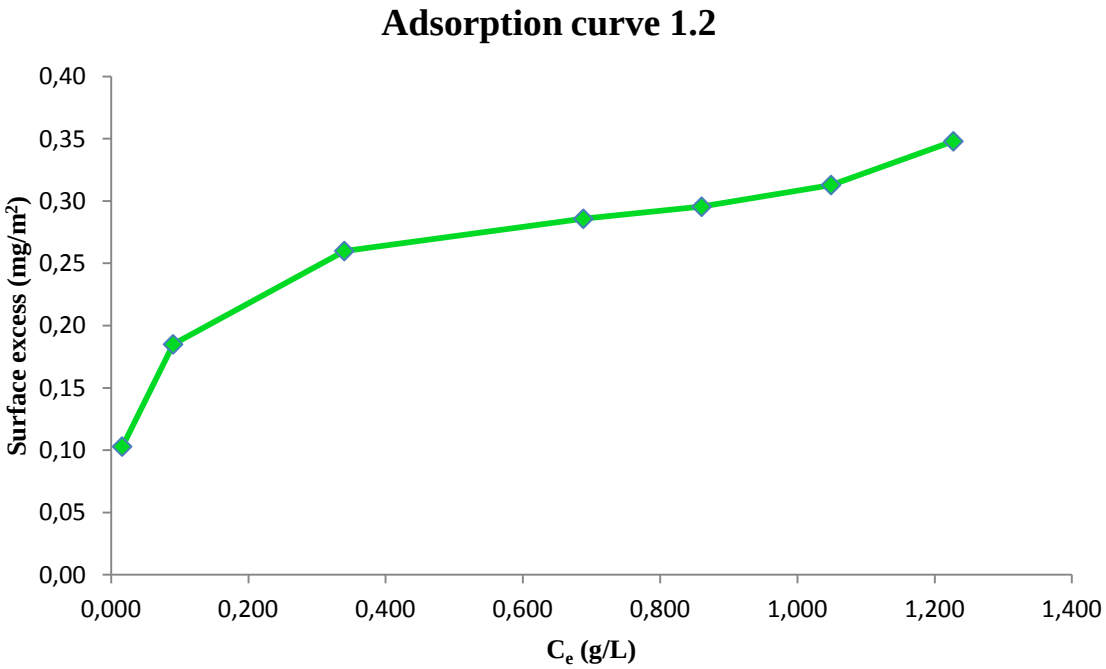

Figure 6-17: Surface excess plotted against equilibrium concentration to achieve an adsorption curve for procedure 1.2.

The adsorption curves from procedure 1.1 (blue) and 1.2 (green) are compared in figure 6-18. The curves show similar trends, especially in the beginning of the graphs. At approximately 0,90 g/L, the green curve continues to increase and the blue starts to decline. The difference in trend at the end can be an uncertainty in the experimental work.

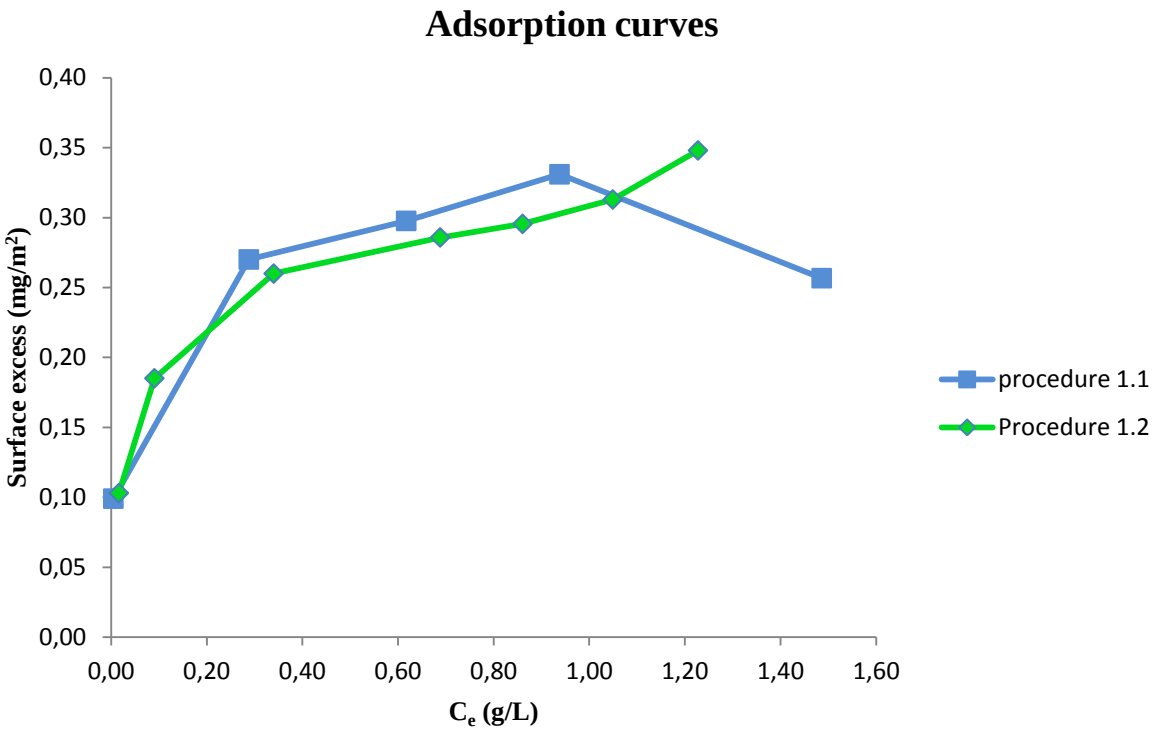

Figure 6-18: A comparison between the adsorption curves from procedure 1.1 (blue) and 1.2 (green).

7. Conclusions

The commercial particles were tested with respect to particle size and surface area, and were found not to fulfil the requirements for studying adsorption of model NA. The size of the particles was estimated to be 3,3 μm, and the specific surface area was calculated to be 1,4 m^2/g. The particle size is too big, thus the surface area is too small.

Therefore, synthesis of new particles was required. Fe_3O_4 magnetic nanoparticles (MNP) were successfully synthesized by co-precipitation, and coated with a silica layer via a sol-gel approach. The synthesized MNP had magnetic properties, and were attracted when the magnetic field was applied. The MAG1 particles were difficult to separate from the liquid, and particles were lost in the washing stages. The yield was 72 %, which implies a considerable loss of MNP. The MAG2 particles were much easier to separate, and had a yield of 109 %. The coating of the MNP with a silica layer had a satisfying yield from 90 % to 102 % for all three batches, which was reflected in the good separation ability from the liquid. The crystallinity of the Fe_3O_4 MNP was found by X-ray diffraction (XRD), and had a good comparability with the standard Fe_3O_4 values. Standards for other iron oxides were also compatible. The XRD peaks were also used to calculate the average particle size of the MAG1 particles, and the size was estimated to be 12 nm. The size estimate for MAG1 was supported by the same calculated size from XRD of SiO_2MAG1, since the SiO_2 layer is amorphous. The diameter was used to estimate the specific surface area of MAG1, and was found to be 98 m^2/g. They were then characterized by gas adsorption analysis, which enabled the measurement of the specific surface area. The Fe_3O_4 MNP and Fe_3O_4/SiO_2 MNP had a large specific surface area of approximately 100 m^2/g, especially compared to the low values of the commercial particles. The measured specific surface area of MAG1 with gas adsorption was very close to the estimated value from the XRD measurements.

The silica covered MNP were used for studying NA adsorption in octane. The model NA were adsorbed from octane, and two absorption curves with similar trends were obtained. The adsorption curves increased in the start and then levelled out from concentration at approximately 0,2 g/L to 0,9 g/L NA in octane. Thereafter, adsorption curve 1.2 increases and was recognized to be most reliable.

From that we could conclude that the designed nanoparticles are suitable for carrying out the proposed experiments and for future surface modifications. Functionalization of the silica covered MNP is the next step in studying adsorption of NA from the model oil and real crude

oil systems. In the current work, extraction of the model NA was carried out from the organic solvent. For the future experiments, the attention should be given to other types of particles (Janus and hydrophilic), making it possible to extract NA from different phases (water or oil/water interfaces). Janus particles are nanoparticles that have a surface with two or more physical properties (Li, et al., 2011). They can for example have both hydrophilic and hydrophobic properties, making it possible for the particles to stay at the oil/water interface and adsorb NA. This property is especially topical for the NA, since both the Janus particles and the NA would then be amphiphilic. Amino-functionalization of the silica-coated particles seems to be one of the more promising methods and shall significantly improve adsorption capacity of the particles compared to the silica-coated ones. A treatment shall also be developed to safely recover the particles and reuse them for further extractions.

8. References

Adamson, A. W., 1982. *Physical chemistry of surfaces.* 4th edition ed. New York: John Wiley and Sons.

Anderson, K. et al., 2013. Removal of naphthenic acids from crude oil using amino acid ionic liquids. *Fuel*, Issue 108, pp. 715-722.

Aske, N., 2002. *Characterisation of crude oil components, asphaltene aggregation and emulsion stability by means of near infrared spectroscopy and multivariate analysis,* Trondheim: Norwegian University of Science and Technology.

Bates, E. D., Mayton, R. D., Ntai, I. & Davis, J. H., 2002. CO2 Capture by a Task-Specific Ionic Liquid. *Journal of the american chemical society*, 19 January, pp. 926-927.

Baugh, T. D., Grande, K. V., Mediaas, H. & Vindstad, J. E., 2005. *The discovery of high-molecular-weight naphthenic acids (ARN acid) responsible for calcium naphthenate deposits,* Aberdeen, UK: SPE international.

Bini, R. A. et al., 2011. Synthesis and functionalization of magnetite nanoparticles with different. *Journal of Magnetism and Magnetic Materials*, 26 August, pp. 534-539.

Brandal, Ø., 2005. *Interfacial (o/w) properties of naphthenic acids and metal naphthenates, naphthenic acid characterization and metal naphthenate inhibition,* Trondheim: Norwegian University of Science and Technology.

Butter, K., Philipse, A. P. & Vroege, G. J., 2002. Synthesis and properties of iron ferrofluids. *Journal of Magnetism and Magnetic Materials*, pp. 1-3.

Clemente, J. S. & Fedorak, P. M., 2005. *A review of the occurrence, analyses, toxicity and biodegradation of naphthenic acids,* Edmonton: University of Alberta, Department of biological sciences.

Cole-Parmer, 2015. *Seeing the Light: An Overview of Visible and UV-VIS Spectroscopy.* [Online]
Available at: http://partners.coleparmer.com/techinfo/techinfo.asp?htmlfile=Overview_Visible_UV_VIS_S

pectroscopy.htm&ID=1396
[Accessed 3 June 2015].

Collins, I. R., Plechkova, N. V. & Anderson, K., 2007. *Process for removing sulfur-containing acids from crude oil.* Belfast, Patent No. WO 138307.

Deng, Y. H. et al., 2005. Investigation of formation of silica-coated magnetite nanoparticles via sol-gel approach. *Colloids and surfaces A: Physiochemical and engineering aspects,* 15 July, pp. 87-93.

Duncum, S. N. & Osborne, C. G., 2002. *Process for deacidifying a crude oil system.* London, Patent No. 6,464,859.

Engen, W. v., 2013. *Micromagnetism, nanomagnetism: magnetic behaviour on a small scale.* Eindhoven: Eindhoven University of Technology.

Euliss, L. E. et al., 2003. Cooperative Assembly of Magnetic Nanoparticles and Block Copolypeptides in Aqueous Media. *Nano Letters*, 6 September, pp. 1489-1493.

Fultz, B. & Howe, J. M., 2013. Diffraction and the X-ray powder diffractometer. In: *Transmission electron microscopy and diffractometry of materials.* Fourth edition ed. s.l.:Springer, pp. 1-57.

Ganichenko, L. G., Kiselev, V. F. & Krasil`nikov, K. G., 1959. *Dokl. Akad. Nauk S.S.S.R.*, Issue 125, p. 1277.

Gillespie, R. D. & Arena, B. J., 1995. *Passing feedstock through a bed of certain metal oxide solid solutions related to hydrotalcites.* Des Plaines, IL, Patent No. US 5.389.240.

Gupta, A. K. & Gupta, M., 2005. Synthesis and surface engineering of iron oxide nanoparticles for biomedical applications. *Biomaterials*, 26 June, pp. 3995-4021.

Halbert, T. R., Riley, K. L., Trachte, K. L. & Vannauker, D. L., 1999. *Process for reduction of total acid number in crude oil.* s.l. Patent No. 5.910.242.

Havre, T. E., 2002. *Formation of calcium naphthenate in water/oil systems, naphthenic acid chemistry and emulsion stability,* Trondheim: Norwegian University of Science and Technology.

Hiemenz, P. C. & Rajagopalan, R., 1997. *Principles of colloid and surface chemistry.* Third edition ed. Boca Raton: CRC press.

Huang, M., Zhao, S., Li, P. & Huisingh, D., 2005. *Removal of naphthenic acid by microwave,* s.l.: Elsevier.

Hyeon, T., 2003. Chemical synthesis of magnetic nanoparticles. *Chemical communications*, 21 April, pp. 927-34.

Hyeon, T. et al., 2001. Synthesis of highly crystalline and monodisperse maghemite nanocrystallites without a size-selection process. *Journal of the American Chemical Society*, 26 December, pp. 12789-801.

Igwebueze, C., Oduola, L. & Smith, O., 2013. *Calcium naphthenate solid deposit identification and control in offshore nigerian fields.* The Woodlands, Texas, SPE international.

Ingle, J. D. & Crouch, S. R., 1988. *Spectrochemical analysis.* 1. edition ed. New Jersey: Prentice hall.

Jiles, D., 1998. Magnetic fields. In: *Introduction to Magnetism and magnetic materials.* 2.nd ed. Boca raton: CRC Taylor & Francis, pp. 3-32.

Kannel, P. & Gan, T., 2012. *Naphthenic acids degradation and toxicity mitigation in tailings wastewater systems and aquatic environments: a review,* Edmonton: Journal of environmental science and health. Part A..

Katz, B. J. & Robison, V. D., 2006. Oil quality in deep-water settings: Concerns, perceptions, observations and reality. *AAPG*, June, Issue 90, pp. 909-920.

Kelland, M. A., 2009. Control of Naphthenate and Other Carboxylate Fouling. In: T. &. F. group, ed. *Production chemicals for the oil and gas industry.* Boca Raton: CRC Press, pp. 189-193.

Keller, J. U. & Staudt, R., 2006. Chapter 1: Basic concepts. In: *Gas adsorption equilibria: Experimental methods and asorption isotherms.* Boston: Springer Science & Business Media, pp. 17-72.

Kim, D. K., Mikhaylova, M., Zhang, Y. & Muhammed, M., 2003. Protective Coating of Superparamagnetic Iron Oxide Nanoparticles. *Chemistry of materials*, 22 March, pp. 1617-1627.

Kiselev, A. V. & Shikalova, I. V., 1970. Adsorption of hydrocarbons from solutions on aerosols and carbon blacks. *Colloid Journal (Transl. of Zollodn. ZH),* Issue 32, p. 588.

Kobayashi, Y. et al., 2003. Preparation and properties of silica-coated cobalt nanoparticles. *The Journal of Physical Chemistry B*, 28 February, pp. 7420-7425.

Krishnan, A., Siedlecki, C. A. & Vogler, E. A., 2003. Traube-Rule Interpretation of Protein Adsorption at the Liquid−Vapor Interface. *Langmuir*, 29 October, Issue 19, pp. 10342-10352.

Langford, J. I. & Wilson, A. J., 1978. Scherrer after sixty years: A survey and some new results in the determination of crystallite size. *Journal of applied crystallography*, April, pp. 102-113.

Laredo, G. C., Altamirano, E. & De los Reyes, J. A., 2003. Inhibition effects of nitrogen compounds on the hydrogensulfurization of dibenzothiophene: Part 2. *Applied catalysis A: General*, 10 April, pp. 207-214.

Laredo, G. C., Lopez, C. R., Alvarez, R. E. & Cano, J. L., 2004. Naphthenic acids, total acid number and sulfur content profile characterization in Isthmus and Maya crude oils. In: *Fuel.* 83 ed. San Bartolo Atepehuacán: s.n., pp. 1689-1695.

Lawrence, M. J. & Rees, G. D., 2000. Microemulsion-based media as novel drug delivery systems. *Advanced drug delivery reviews*, 6 December, pp. 89-121.

Li, D. F., Josephson, D. P. & Stein, P. A., 2011. Colloidal Assembly: The Road from Particles to Colloidal Molecules and Crystals. *Angewandte Chemie International Edition*, 10 January, Issue Issue 2, pp. 360-388.

Liu, X., Guan, Y., Ma, Z. & Liu, H., 2004. Surface modification and characterization of magnetic polymer nanospheres prepared by miniemulsion polymerization. *Langmuir*, 9 November, pp. 10278-82.

Lu, A. H. et al., 2005. Highly stable carbon-protected cobalt nanoparticles and graphite shells. *Chemical Communications*, 7 January, pp. 98-100.

Macintyre, S. A., 1999. Magnetic field measurement. In: J. G. Webster, ed. *The measurement, instrumentation and sensors handbook.* s.l.:CRC Press.

Mackenzie, A. S., Wolff, G. A. & Maxwell, J. R., 1983. Fatty acids in biodegraded petroleums. Possible origins and significance. In: M. Bjorøy, ed. *Advances in Organic Geochemistry 1981*. Chichester, UK: John Wiley, pp. 637-649.

McMurry, J., 2008. *Organic chemistry.* 7th edition ed. London: Thomson.

Mediaas, H., Grande, K. V. & Vindstad, J. E., 2007. *Efficient management of calcium naphthenate deposition at oil fields.* s.l.: TEKNA; Statoil.

Neveu, S., Bee, A., Robineau, M. & Talbot, D., 2002. Size-selective chemical synthesis of tartrate stabilized cobalt ferrite ionic magnetic fluid. *Journal of Colloid and Interface Science,* Issue 255, pp. 293-298.

Nunez, N. O. et al., 2004. Yttria-Coated FeCo Magnetic Nanoneedles. *Chemistry of materials*, 17 July, pp. 3119-3124.

Parfitt, G. D. & Rochester, C. H., 1983. Adsorption of small molecules. In: *Adsorption from solution at the solid/liquid interface.* London: Academic press, pp. 3-41.

Park, J. et al., 2004. Ultra-large-scale syntheses of monodisperse nanocrystals. *Nature materials,* Issue 3, pp. 891-895.

Pathak, A. K. & Kumar, T., 1995. Study of indigenous crude oil emulsions and their stability. In: *Proceedings of PETROTECH-95.* New Dehli: Technology trends in oil industry.

Payne, M. A., 1981. SI and Gaussian cgs units, conversions and equations for use in geomagnetism. *Physics of the Earth and Planetary Interiors,* December, Issue 26, pp. 10-16.

Puntes, V. F., Krishan, K. M. & Aliviatos, A. P., 2001. Colloidal nanocrystal shape and size control: The case of cobalt. *Science,* Issue 291, pp. 2115-2117.

Reinsel, M. A., Borkowski, J. J. & Sears, J. T., 1994. Partition Coefficients for Acetic, Propionic, and Butyric Acids in a Crude Oil/Water System. *Journal of chemical and engineering data*, July, pp. 513-516.

Rodriguez, R. A. & Ubbels, S. J., 2007. Understanding naphthenate salt issues in oil production. *World Oil*, 228(8), pp. 143-145.

Rousseau, G., Zhou, H. & Hurtevent, C., 2001. *Calcium carbonate and naphthenate mixed scale in deep-offshore fields,* Aberdeen, UK: SPE Oilfield Scale Symposium.

Sahoo, Y. et al., 2001. Alkyl Phosphonate/Phosphate Coating on Magnetite Nanoparticles: A Comparison with Fatty Acids. *Langmuir*, 11 December, pp. 7907-7911.

Scaled solutions LTD, 2014. *Naphthenates.* [Online] Available at: http://www.scaledsolutions.com/Innovation%20R%20and%20D/Naphthenates [Accessed 8 December 2014].

Schüth, F., Lu, A. -H. & Salabas, E. L., 2007. Magnetic nanoparticles: synthesis, protection, functionalization and application. *Angewandte Chemie: International edition*, 12 February, Issue 46, pp. 1222-1244.

Sheperd, A. G., 2008. *A Mechanistic Analysis of Naphthenate and Carboxylate Soap-Forming Systems in Oilfield Exploration and Production,* Edinburgh: Heriot-Watt University.

Shi, S., Xiao, Q. & Chen, A., 2002. Study on the Synthesis and Application of Naphthenic Acid Hydroxyalkylamides. *Coal chemical industry*, Issue 1, pp. 15-18.

Sjöblom, J. et al., 2003. Our current understanding of water-in-crude oil emulsions. Recent characterization techniques and high pressure performance.. *Advances in Colloid and Interface Science*, pp. 399-473.

Sobal, N. S. et al., 2002. Synthesis and structure of colloidal bimetallic nanocrystals: The non-alloying system Ag/Co. *Nano Letters*, 3 May, pp. 621-624.

Speight, J. G., 1999. *The chemistry and technology of petroleum.* Third edition ed. New York: Marcel Dekker.

Statoil, 2007. *Naphthenate chemistry breakthrough.* [Online] Available at: http://www.statoil.com/en/technologyinnovation/refiningandprocessing/oilrefining/naphthenatechemistrybreakthrough/pages/default.aspx
[Accessed 24 Oktober 2014].

Sun, S. et al., 2000. Monodisperse FePt nanoparticles and ferromagnetic FePt nanocrystal superlattices. *Science,* Issue 287, pp. 1989-1992.

Traube, J., 1891. Ueber die Capillaritätsconstanten organischer Stoffe in wässerigen Lösungen. *Annalen*, Issue 265, pp. 27-55.

Tsang, S. C. et al., 2004. Magnetically separable, carbon-supported nanocatalysts for the manufacture of fine chemicals. *Angewandte Chemie International Edition*, 25 October, pp. 5645-9.

Ubbels, S. J., 2004. Preventing naphthenate stabilized emulsions and naphthenate deposits during crude oil processing. In: *Proceedings from the 5th international conference on petroleum phase behaviour and fouling.* s.l.:s.n.

Vindstad, J. E. et al., 2003. *Fighting naphthenate deposition at the Heidrun field.* Aberdeen, SPE international.

Wang, J. et al., 2010. Amino-functionalized Fe3O4@SiO2 core shell magnetic nanomaterial as a novel adsorbent for aqueous heavy metal removal. *Journal of colloid and interface science*, 7 May, pp. 293-299.

Wang, X., Zhuang, J., Peng, Q. & Li, Y., 2005. A general strategy for nanocrystal synthesis. *Nature*, 1 September, pp. 121-124.

Wang, Y. Z., Liu, Y. P. & Liu, C. G., 2008. Removal of Naphthenic Acids of a Second Vacuum. *Petroleum science and technology*, 21 July, pp. 1424-1432.

Wilks, J., 2010. *Free radical chemistries at the surface of electronic materials,* Denton, Texas: University of North Texas digital library.

Willis, A. L., Turro, N. J. & O'Brien, S., 2005. Spectroscopic characterization of the surface of iron oxide nanocrystals. *Chemistry of materials,* Issue 17, pp. 5970-5975.

Xie, L. et al., 2013. Application of functionalized magnetic nanoparticles in sample preparation. *Analytical and bioanalytical chemistry*, 14 September, pp. 377-399.

Zhang, A. et al., 2005. Naphthenic acid removal from crude oil through catalytic decarboxylation on magnesium oxide. *Science direct*, 9 March, pp. 103-109.

Zhang, C. et al., 2007. Silica- and alkoxysilane-coated ultrasmall superparamagnetic irod oxide particles: A promising tool to label cells for magnetic resonance imaging. *Langmuir*, pp. 1427-1434.

Zhang, J. et al., 2006. Supported Absorption of CO2 by Tetrabutylphosphonium Amino Acid Ionic Liquids. *Chemistry - A European journal*, 10 March, pp. 4021-4026.

Zhang, X. et al., 2011. Modifying the surface of Fe3O4/SiO2 magnetic nanoparticles with C18/NH2 mixed group to get an efficient sorbent for anionic organic pollutants. *Journal of colloid and interface science*, 22 June, pp. 107-112.

9. Appendices

9.1 Instruments

All instruments are listed by production company and model.

Hardware

Production company	*Model*
Amazing magnets	D500P, size: 2” × 0.5” Grade: N40
Bruker	D8 Advance DaVinci X-ray diffractometer
Eppendorf	Centrifuge 5810
Hellma Analytics	Precision cells made of Quartz Suprasil ®
Heidolph	Laborota 4003 Rotavapor, pump: laboxact
Heidolph	MR 3004 Safety
IKA	HS 501 digital laboratory shaker
Malvern Instruments	Zetasizer Nanoseries, Nano ZS
Media Cybernetics	CoolSNAP-Pro Monochrome
Micromeritics Instrument Corporation	TriStar 3000 Gas Adsorption Analyzer
Nikon	Eclipse ME600 microscope
Shimadzu	UV – 2401PC, UV-vis Recording Spectrophotometer

Software

Production company	*Version*
Bruker	DIFFRAC.EVA V4.0
Media Cybernetics	Image pro plus 5.0
Shimadzu	UVProbe 2.10
Micromeritics Instrument Corporation	Tristar 300 software Version 6.04

9.2 Tables

Table 9.1: Calibration curve 1 for NA in octane. Calculated concentration and measured absorbance at 243 nm. The stock solution is 0,14 g/L NA for solution 1-5, and 2,1 g/L NA for solution 6-7.

Sample	Stock (g)	Octane (g)	Concentration (g/L)	Absorbance at 243 nm
Blank	0,0000	5,0000	0,0000	0,00031
1	0,6319	4,4405	0,0177	1,37415
2	1,0147	9,0872	0,0143	1,0656
3	0,1395	4,8020	0,0040	0,22763
4	0,5080	10,9643	0,0063	0,43227
5	0,7678	9,6239	0,0105	0,80193
6	0,0490	9,9514	0,0102	0,80997
7	0,0830	9,9383	0,0172	1,43459

Table 9.2: Calibration curve 2 for NA in octane. Calculated concentration and measured absorbance at 243 nm. The stock solution is 1,00 g/L NA.

Sample	Stock (g)	Octane (g)	Concentration (g/L)	Absorbance at 243 nm
Blank	0,0000	7,0300	0,0000	-0,00072
1	0,0326	6,9796	0,0046	0,35580
2	0,0533	6,9866	0,0076	0,58163
3	0,0530	6,9902	0,0075	0,57703
4	0,0725	6,9655	0,0103	0,80559
5	0,0865	6,9455	0,0123	0,96193
6	0,1031	6,9367	0,0146	1,15076
7	0,1154	6,9002	0,0164	1,29002
8	0,1239	6,8972	0,0176	1,38167

Table 9.3: Measured mass of SiO_2MAG1.2 with calculated total surface area, mass of octane, mass of stock (2,09 g/L), total concentration of NA and total volume before adsorption for 24 hours (Test procedure)

Sample	MNP (mg)	Surface (m^2)	Octane (g)	Stock (g)	C_O (g_{NA}/L)	V (L)
Blank	0,0	0,0	7,5424	0,0000	0,000	-
Reference	43,3	5,3	7,1111	0,0000	0,000	-
1	41,5	5,0	6,8336	0,4678	0,134	0,0104
2	45,7	5,6	6,3356	0,7066	0,209	0,0100
3	41,7	5,1	5,6181	1,4639	0,431	0,0101
4	41,2	5,0	4,9624	2,1170	0,624	0,0101
5	40,7	4,9	4,2613	2,8547	0,837	0,0101
6	42,0	5,1	3,8409	3,7876	1,036	0,0109
7	41,7	5,1	2,8442	4,2452	1,250	0,0101
8	43,7	5,3	2,1276	5,1081	1,474	0,0103
9	41,8	5,1	1,4458	5,6442	1,662	0,0101
10	41,6	5,1	0,7288	6,3945	1,874	0,0101

Table 9.4: Measured mass of SiO_2MAG1.2 with calculated total surface area, mass of octane, mass of stock (1,99 g/L), total concentration of NA and total volume before adsorption for 24 hours (procedure 1.1)

Sample	MNP (mg)	Surface (m^2)	Octane (g)	Stock (g)	C_O (g_{NA}/L)	V (L)
Blank	0,0	0,0	3,5150	0,0000	0,000	-
Reference	80,9	9,8	3,5261	0,0000	0,000	-
1	83,0	10,1	3,1599	0,3617	0,204	0,0050
2	78,6	9,6	2,1669	1,4350	0,791	0,0051
3	79,8	9,7	1,4234	2,1234	1,189	0,0050
4	80,7	9,8	0,7166	2,8169	1,584	0,0050
5	80,6	9,8	0,0000	3,5337	1,986	0,0050

Table 9.5: Measured mass of SiO_2MAG2.1 with calculated total surface area , mass of octane, mass of stock (1,95 g/L), total concentration of NA and total volume before adsorption for 24 hours (procedure 1.2)

Sample	MNP (mg)	Surface (m^2)	Octane (g)	Stock (g)	C_O (g_{NA}/L)	V (L)
Blank	0,0	0,0	3,5150	0,0000	0,000	-
Reference	83,0	8,7	3,5522	0,0000	0,000	-
1	82,1	8,6	3,1652	0,3488	0,193	0,0050
2	79,5	8,3	2,8208	0,7206	0,397	0,0050
3	80,6	8,4	2,1127	1,4059	0,779	0,0050
4	79,9	8,4	1,4167	2,1082	1,166	0,0050
5	80,6	8,4	1,0646	2,4546	1,359	0,0050
6	77,5	8,1	0,7084	2,8124	1,557	0,0050
7	78,8	8,3	0,4501	3,567	1,730	0,0057

9.3 UV spectroscopy

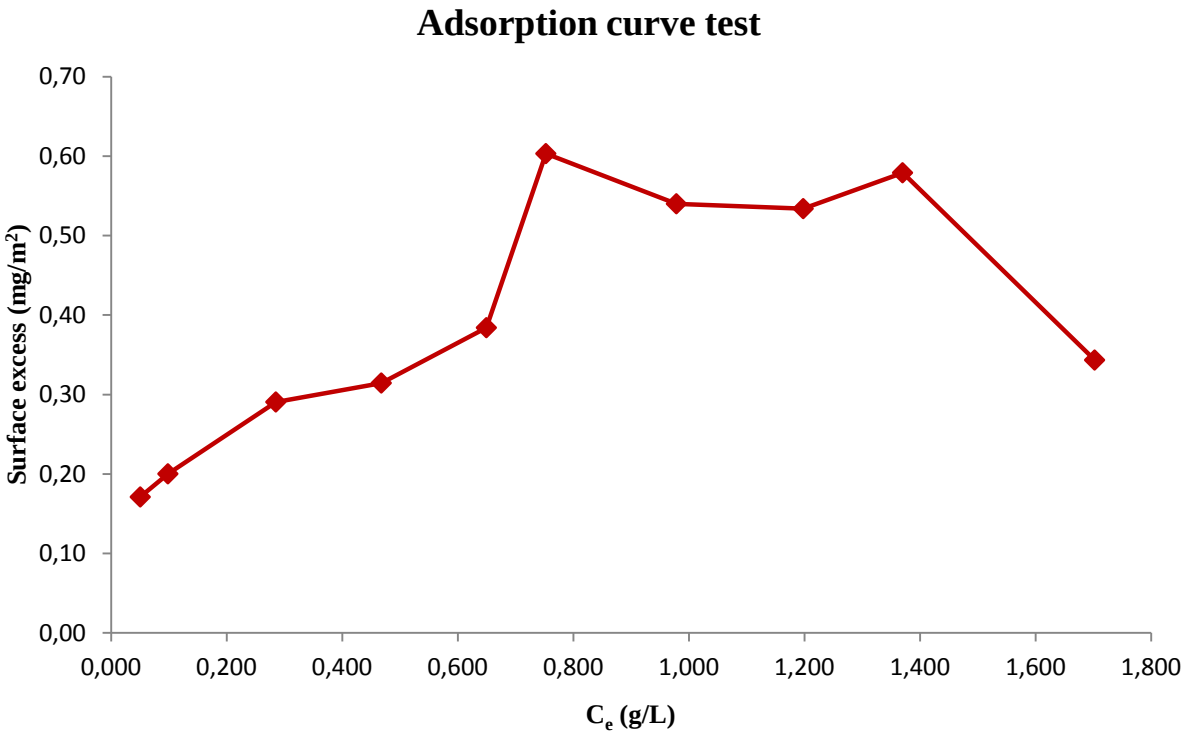

Figure 9-1: Surface excess plotted against equilibrium concentration to achieve an adsorption curve for the test procedure.

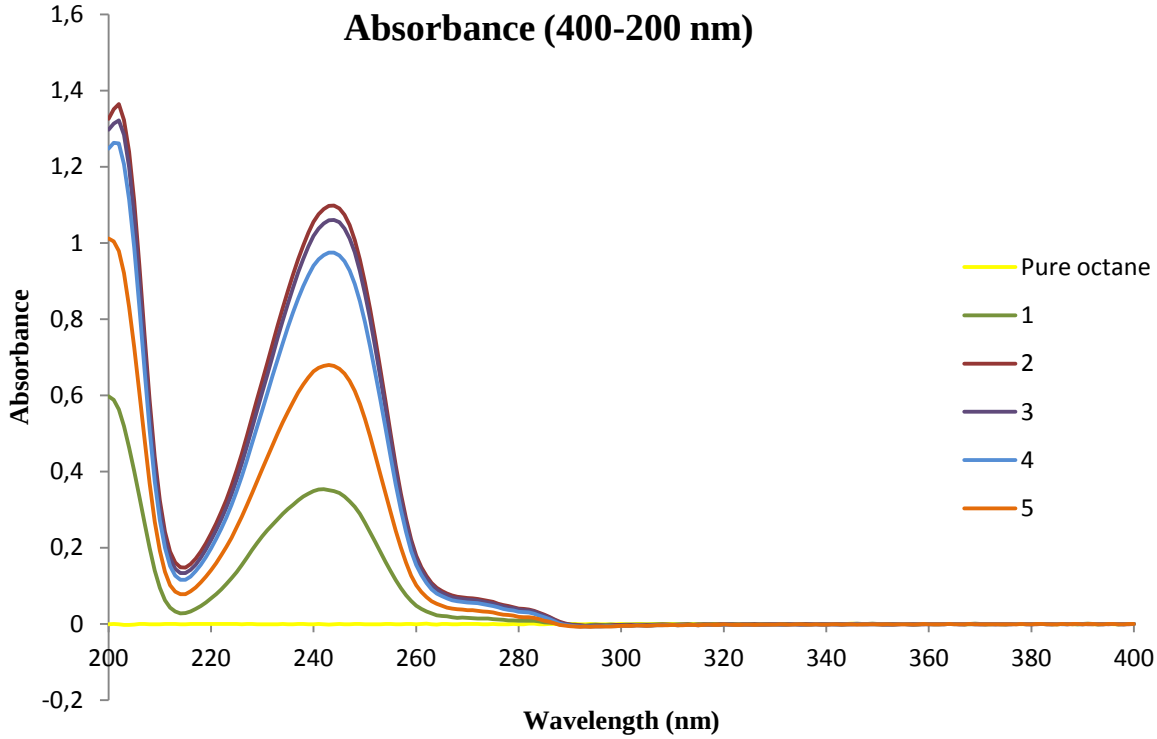

Figure 9-2: Absorbance measured at wavelength 400 to 200 nm for all samples (1-5) and pure octane from adsorption procedure 1.1 (SiO_2MAG1.2).

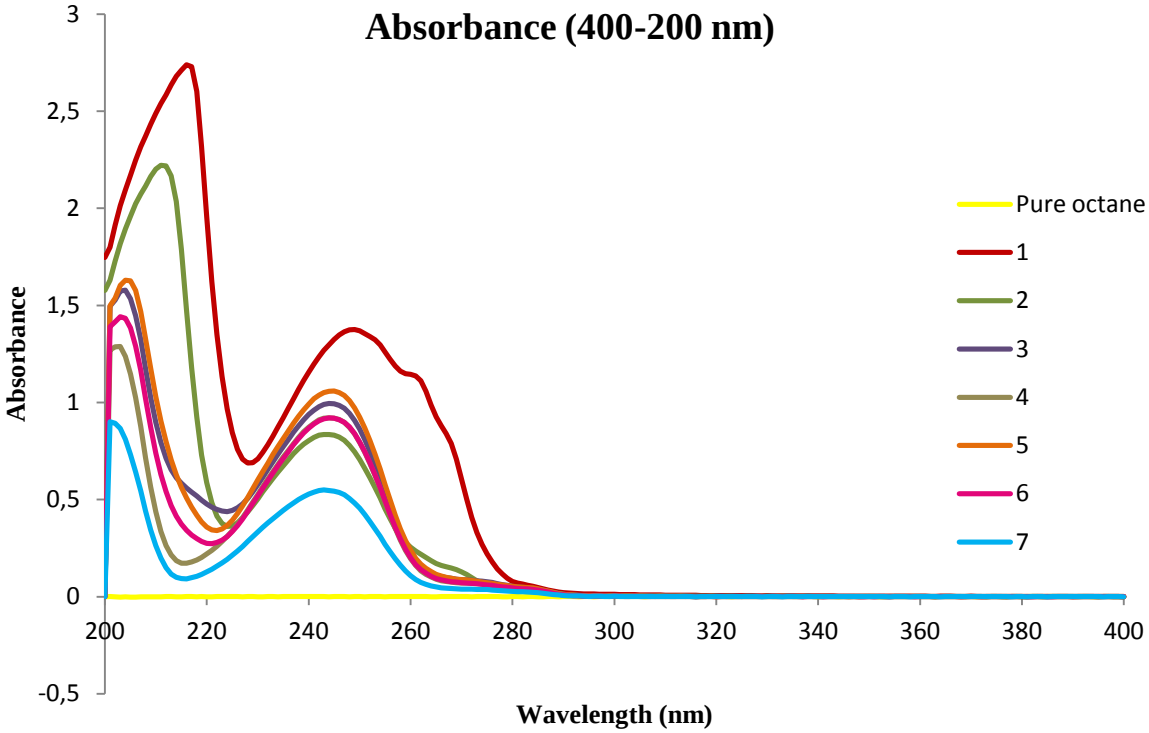

Figure 9-3: Absorbance measured at wavelength 400 to 200 nm for all samples (1-7) and pure octane from adsorption procedure 1.2 (SiO_2MAG2.1).